Referential communication in heterogeneous communities of pre-trained visual deep networks

Matéo Mahaut *mateo.mahaut@upf.edu*
Francesca Franzon *francesca.franzon@upf.edu*
Roberto Dessì *roberto.dessi@upf.edu*
Universitat Pompeu Fabra

Marco Baroni *marco.baroni@upf.edu*
Universitat Pompeu Fabra and ICREA

Reviewed on OpenReview: `https://openreview.net/forum?id=8L3khbpUJL`

Abstract

As large pre-trained image-processing neural networks are being embedded in autonomous agents such as self-driving cars or robots, the question arises of how such systems can communicate with each other about the surrounding world, despite their different architectures and training regimes. As a first step in this direction, we systematically explore the task of *referential communication* in a community of heterogeneous state-of-the-art pre-trained visual networks, showing that they can develop, in a self-supervised way, a shared protocol to refer to a target object among a set of candidates. This shared protocol can also be used, to some extent, to communicate about previously unseen object categories of different granularity. Moreover, a visual network that was not initially part of an existing community can learn the community's protocol with remarkable ease. Finally, we study, both qualitatively and quantitatively, the properties of the emergent protocol, providing some evidence that it is capturing high-level semantic features of objects.

1 Introduction

As state-of-the-art vision-processing deep networks start being deployed as components of real-life autonomous or semi-autonomous systems, the question arises of how such systems can communicate about the surrounding visual world, as seen through the lenses of their respective core visual components. Consider for example two industrial robots produced by different companies, or two self-driving cars from different makers, that need to coordinate about objects in their environment. One might be powered, say, by a ResNet convolutional net (He et al., 2016) trained on the ImageNet visual recognition challenge (Russakovsky et al., 2015), whereas the other might use a Vision Transformer trained with a self-supervised algorithm (Dosovitskiy et al., 2021; Caron et al., 2021). The set of object labels known to the two nets might differ (if labels are present at all), and, even when they coincide, the underlying categorization algorithms of the two nets might label the same object in different ways. Moreover, the original label set might not suffice to discriminate objects in the environment. For example, both nets might have been trained to categorize certain objects as *dogs*, but the current situation requires them to distinguish among multiple *dog* instances, or to denote an unfamiliar mammal neither network encountered at training time. Next, consider the scenario where a third system, relying on yet another visual network, is added to an existing "community" of systems that are already able to communicate. Do we need to develop a new communication protocol, or can the new agent quickly adapt to the one already in use? Could we eventually derive a universal protocol that any network-powered system could rapidly acquire? Note that, in the scenarios we are considering, the internal weights of the visual components might not be accessible for fine-tuning the network community as a single

system, and, even if they were, this might be extremely costly or undesirable, as the core functionalities of the networks should not be altered.

We begin to tackle the challenges we outlined by studying whether a set of diverse pre-trained visual networks, augmented with a light interface layer, can develop a shared protocol when faced with the core communicative task of *referring to a specific object* among a set of candidates (Skyrms, 2010). We are inspired by recent work on *deep net emergent communication* (Lazaridou & Baroni, 2020). However, we adopt a different perspective with respect to this line of research. Instead of designing *ad-hoc* architectures specifically optimized on the communication task, we look at emergent referential communication in communities of multiple pre-trained networks with heterogeneous architectures and training histories. We emphasize that our goal is to study the ability of heterogeneous networks to converge on a common referent. The full embodiment of such networks in autonomous agents that interact in a real-life environment involves a large number of challenges that we are not tackling here.

After reviewing related work (Section 2) and presenting our general setup (Section 3), we delve into our experiments in Section 4. First, in Section 4.1, we show that it is indeed possible for sets of heterogeneous pre-trained networks to successfully converge on a referent through an induced communication protocol. In Section 4.2, we study *referential generalization*, showing that the developed protocol is sufficiently flexible that the networks can use it to refer to objects that were not seen during the training phase (the "unfamiliar mammal" case we discussed above), as well as to tell apart distinct instances of the same object (the "distinguishing between different dogs" case above). We further show that the networks can successfully communicate about images from new datasets that were not used during communication training. In Section 4.3, we consider instead *agent generalization*. We show that, given a community of networks that have been trained to communicate, it is faster for a new pre-trained network with a different architecture, training objective or training corpus to acquire the existing community protocol, than for the enlarged community to develop a new protocol from scratch. This suggests that we could use a small set of networks to develop a "universal" protocol, that can then be taught in a supervised way to new networks that require the envisaged communication functionality. In Section 4.4 we offer some qualitative and quantitative insights into the protocol, suggesting that the network populations have developed a single shared code, that is not (only) referring to low-level image features, but also to higher-level semantic concepts, which we identify using sparse autoencoders (SAEs). The Conclusion (Section 5) takes stock of what we found, and discusses the way ahead.

The main contributions of this paper are as follows:

- We introduce and motivate the task of referential communication between pre-trained heterogeneous visual networks;
- We show that a low-dimensional communication layer trained in a self-supervised way is sufficient to achieve high performance on the task, given a variety of different networks tested on in-domain data;
- We show that the learned communication protocol partially transfers to out-of-domain data, including new and more granular referents than those seen at training time;
- We show that a new pre-trained network can successfully and efficiently learn an existing protocol;
- Quantitative and qualitative analysis of the protocol suggests that it is encoding high-level semantic features.

2 Related work

Deep net emergent communication While there is a long tradition of work on communication emergence in communities of generic computational agents (e.g., Cangelosi & Parisi, 2002; Christiansen & Kirby, 2003; Wagner et al., 2003; Nolfi & Mirolli, 2020; Steels, 2012), there has recently been interest in the specific topic of *deep-net-based* emergent communication, with the aim to develop a protocol for autonomous information exchange between modern deep neural networks (Lazaridou & Baroni, 2020).

Since the ability to refer to a specific object in a shared environment is seen as one of the core building blocks of communication, many studies in this area have focused on the *referential game* setup, where a sender network must send a message to a receiver network to help it discriminate a target object among a set of candidates (e.g., Lazaridou et al., 2017; Havrylov & Titov, 2017; Dessì et al., 2021).

Inspired by human language, most work focusing on the referential game has been exploring a *discrete* communication setup in which the sender produces a symbol or a sequence of symbols. On the other hand, a continuous channel is often preferred in scenarios where agents have to tackle navigation-like tasks in environments featuring relatively few distinct referents (e.g., Foerster et al., 2016; Sukhbaatar et al., 2016; Tieleman et al., 2018; Kim et al., 2019; Singh et al., 2019). Carmeli et al. (2022) have recently shown that continuous communication outperforms discrete communication in the context of the referential game. As discrete communication imposes a non-differentiable bottleneck requiring special optimization techniques, we focus on the more natural continuous setup. We do however explore alternatives involving a discrete channel in Appendix C.

Larger human speaker communities lead to the emergence of better-behaved protocols (e.g., Raviv et al., 2019). Many studies have assessed the impact of community size in deep network language emergence (e.g., Tieleman et al., 2018; Cogswell et al., 2019; Graesser et al., 2019; Li & Bowling, 2019; Ren et al., 2020). It appears that community-based training leads to desirable properties such as systematicity and ease of learning, at least when relatively small populations of homogeneous agents are considered. However, Rita et al. (2022) and Chaabouni et al. (2022) have recently shown that, in large-scale setups and when appropriate controls are considered, population training by itself does not bring about any special benefit. We are not so much interested in whether population-based training *per se* improves communication, but rather in whether it is possible at all to develop a shared protocol that is usable by multiple heterogeneous pre-trained networks, and easy to learn for new networks added to a community.

In typical population-based emergent communication studies, the networks in the population share the same architecture. Rita et al. (2022) looked at the effect of introducing sources of heterogeneity between senders and receivers, finding that using agents with different learning rates enhances population-based protocols. While encouraging, this result was based on varying a single hyperparameter of otherwise identical networks, still far from our community-of-heterogeneous-networks scenario.

Representation similarity, model stitching and multimodal representation learning Our work touches upon the issue of whether different neural networks share similar representations (e.g., Li et al., 2016; Morcos et al., 2018; McNeely-White et al., 2020; Huh et al., 2024). Some of the work on this topic adopts a method known as "model stitching," which consists in connecting intermediate layers of two models to measure their compatibility (Lenc & Vedaldi, 2019; Bansal et al., 2021). This can be seen a form of model-to-model communication. Moschella et al. (2023); Maiorca et al. (2023), in particular, have recently introduced an unsupervised method that allows heterogeneous encoder and decoder networks to be "stitched" together in a 0-shot manner, based on second-order object representations (objects are represented by their similarities to a set of reference objects). Applying this approach to our referential communication scenario is a possible direction for future work. Research on multimodal representation learning and alignment (e.g., Darvish et al., 2023; Girdhar et al., 2023; Liang et al., 2023; Yu et al., 2024) is also strongly related to our aims. For example, Moayeri et al. (2023) present a cross-visual-model alignment method similar to our communication layer. However, differently from their research line, where the emphasis is on multiple modalities and to train a single system that works across them, we are specifically interested in connecting heterogeneous pre-trained visual models in a light and efficient way, and in studying the properties of the emergent protocol shared by a whole population of such models.

Self-supervised learning for image classification Various self-supervised discriminative training approaches have used objectives similar to our referential game, in order to derive classifiers without relying on annotated data (Chen et al., 2020; Caron et al., 2021). Sometimes the setup is explicitly conceptualized as a multi-agent system (Grill et al., 2020). Some of the questions that are discussed in this field are also relevant for us. For example Lavoie et al. (2023) studied the effect of sparsifying representations into a constrained space, showing it improves generalization on new datatsets (we tried their methodology as an alternative way

to derive discrete message representations in Appendix C, but found it non-competitive in our setup). While there are similarities between our core methodology and self-supervised learning, our aim is fundamentally different: we are not trying to induce an image classifier from scratch without annotated data, but to let distinct pre-trained networks (typically already trained as image classifiers) share information.

Our referential game can also be seen as a content-based image retrieval task, and in this sense our work is related to image retrieval using contrastive objectives (e.g., Wang et al., 2020b; El-Nouby et al., 2021). However, we do not train or fine-tune a full network to improve referent retrieval, but rather train shallow layers overlaid onto frozen networks with different architectures, and our emphasis, again, is on information sharing across networks.

Multi-agent systems More broadly, our work fits into the wider area of multi-agent systems research, specifically cooperative learning and the decentralized POMDP setup (Panait & Luke, 2005; Oliehoek & Amato, 2016), a field in which there is also interest in the problem of optimizing the behavior of a diverse set of cooperating agents (e.g., Canaan et al., 2019). In the multi-agent decentralized learning domain, federated learning (e.g., McMahan et al., 2017; Lim et al., 2020) focuses on leveraging distributed model instances with different data sources to improve training. Like us, this domain studies communication efficiency and convergence of multiple agents (Wang et al., 2020a). However, we do not distribute training among a set of similar networks, focusing instead on multiple agents characterized by strong differences, and their ability to complete a communication task.

3 Setup

3.1 The referential communication game

Inspired by the core communicative task of *reference* (e.g., Skyrms, 2010), in the referential communication game a *sender* is given a target input (e.g., a picture) and issues a message (e.g., a word or, as in our case, a continuous vector). A *receiver* is exposed to a set of inputs, including the target, and must correctly point to the latter based on the message it receives from the sender.

Our sender and receiver are neural networks that include pre-trained and frozen visual modules, plus wrapper components in charge of message passing. We refer to the full interacting systems as *agents*. In each episode of the game, the sender agent receives a target image as input, processes it with its visual module, and outputs a message to the receiver. The receiver gets the message and is presented with a set of candidate images, containing the target and a series of distractors. For every candidate image, the receiver, using its visual module, constructs a representation, which is then compared to a representation of the received message. The receiver selects whichever candidate has the most similar representation to the message. If the selected image matches the target, the episode is successful. Success above chance level is only possible if the receiver learns to correctly interpret the message sent by the sender. Pseudocode for the referential game is presented in Appendix A.

Crucially, task accuracy only depends on target image matching, and does not require any kind of annotation. As such, the communication protocol is entirely learned in a self-supervised way.

Below, we refer to the basic setup, in which a single sender-receiver pair is jointly trained to play the game, as the *one-to-one* setting, further distinguished into *homogeneous* and *heterogeneous* cases, depending on whether the two agents use the same or different visual modules for image processing. To extend the game to the *population* setting, given a population of N senders and receivers, we randomly sample one sender and one receiver at each step to play the game as previously described.

3.2 Agent architectures and training

As mentioned, both sender and receiver are neural networks made up of a frozen vision module and light feed-forward layers used for communication (Fig. 1).

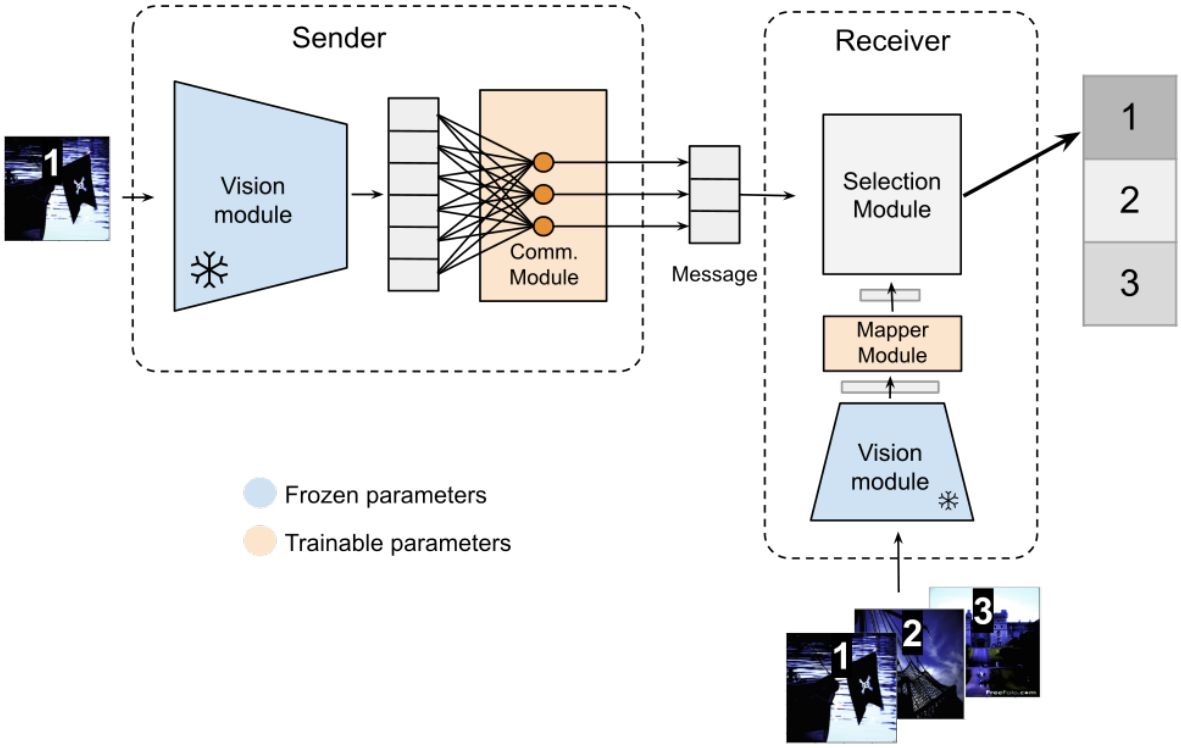

Figure 1: Referential game setup and agent architectures. A target image is input to the sender, that extracts a vector representation of it by passing it through a pre-trained frozen visual network. This vector representation is fed to the feed-forward *Communication Module*, that generates a message consisting of another continuous vector, that is passed as one of the inputs to the Receiver. The receiver also processes each candidate image it gets as input by passing it through a pre-trained frozen visual network (which can have a different architecture from the one of the sender), obtaining a set of vector representations. These are fed to the receiver's *Communication Module*, another feed-forward component that maps them to vectors in the same space as the sender message embedding. The *Selection Module* of the receiver simply consists of a parameter-free cosine similarity computation between the message and each image representation, followed by Softmax normalization. The receiver is said to have correctly identified the target if the largest value in the resulting probability distribution corresponds to the index of the target in the candidate array. Note that no parameters are shared between sender and receiver (except those of the frozen visual modules in the case in which the two agents are using homogeneous visual architectures).

Architecture	Type	Training	Parameters
ResNet152	CNN	Supervised ImageNet1k	60.2M
ResNet50	CNN	Supervised COCO	23.5M
Inception	CNN	Supervised ImageNet1k	27.2M
VGG 11	CNN	Supervised ImageNet1k	132.9M
ViT-B/16	Attention	Supervised ImageNet1k	86.6M
ViT-S/16	Attention	Self-supervised ImageNet1k	21M
Swin	Attention	Supervised ImageNet1k	87.7M

Table 1: Pre-trained visual architectures employed

3.2.1 Pre-trained vision modules

As vision modules, we use widely adopted networks that have freely downloadable parameters (Table 1). We mainly consider architectural variations of networks trained with a supervised classification objective, as this is the most common axis of variation across modern models. In particular, we use both convolutional (*ResNet*: He et al. (2016), *Inception*: Szegedy et al. (2014), *VGG*: Simonyan & Zisserman (2015)) and attention-based networks (*ViT*: Dosovitskiy et al. (2021), *Swin*: Liu et al. (2021)), trained on ILSVRC2012 ImageNet data (Russakovsky et al., 2015). We however also include in our collection a ResNet (from Desai & Johnson (2021)) that was trained on a different dataset, namely COCO (Chen et al., 2015). The latter involves fewer labels as well as stronger data imbalance (Gauen et al., 2017). Finally, we include an attention-based network, DINO (Caron et al., 2021), that was trained on ImageNet, but using a self-supervised objective (denoted by its ViT-S/16 architecture in Table 1). Further pre-trained networks are used in the agent generalization experiments, as briefly discussed in Section 4.3 below: see Table 22 in Appendix M for details.

The weights of the visual models are frozen (in blue in Fig. 1) and they are not modified at any point during our experiments. As output from the vision modules, we use their last layer, before the Softmax non-linearity is applied. Therefore, the vision module takes as input images and outputs vector representations.

While we are interested, by problem definition, in communication between *pre-trained* networks, whose visual processing abilities largely derive from the pre-training phase, in Appendix B we try to assess to what extent emergent discrimination abilities are a simple by-product of pre-training. The results there suggest that this is not the case.

3.2.2 Trainable communication components

The second part of an agent's architecture consists in the layers devoted to handling communication. In both sender and receiver, all communication-related parameters are trainable, as shown in orange in Fig.1.

In the sender, the communication module is a small linear feed-forward layer, with between 6k and 264k parameters. For comparison, the frozen vision modules in Table 1 all have more than 20M parameters. The communication module takes as input the image representation, and outputs a continuous vector we refer to as the *message* emitted by the sender. We ran a hyper-parameter search for message dimensionality (Appendix D). Since we found a ceiling effect, we decided to run all experiments with both the smallest (16) and the largest (64) size that reached peak validation performance. Note that, when we use the term *communication protocol* below, we refer to the deterministic input-conditioned message-emitting policy the sender converges to after training.

In the receiver, the vision module is followed by its own communication module, mappping the former outputs to new, compressed image representations that live in the same space as the message. Following standard practice in the emergent communication literature, the message is compared to the image representations through the parameter-free cosine similarity measure. The receiver communication module is larger than the sender communication component, being composed of two linear layers with a hidden dimension, as we adopted the architecture of Dessì et al. (2021) without further tuning. The number of parameters remains well below that of the pre-trained vision modules. As an example, VGG (132.9M parameters) is the vision

module that has the largest output dimension, and therefore requires the largest communication module, with 8.4 million parameters, still less than 1/10 the number of parameters of the vision module.

Emergent communication research often adopts a discrete channel, as the latter more closely emulates human linguistic communication. We experimented extensively with a discrete interface, as reported in Appendix C. However, as discrete communication does not lead to clear advantages over continuous communication, and it involves a more involved and brittle optimization process, we focus here on the continuous interface we just described.

3.2.3 Training

As the sender-receiver interface is continuous, the whole system can be straightforwardly trained by back-propagating the cross-entropy loss obtained by comparing the receiver output to the ground-truth target.

Batch size is set at 64, the largest value we could robustly fit in GPU memory. As we sample distractors directly from training batches, on each training step the referential game is played 64 times, once with every different image in the batch as target and the other 63 images serving as distractors. All experiments are implemented using the EGG toolkit (Kharitonov et al., 2019)[1]. All parameters needed to reproduce our experiments with the toolkit (both the continuous setup reported here, and the discrete one discussed in Appendix C) can be found in Appendix E. Evidence of training convergence is provided in Appendix F in terms of gradient evolution profiles. Appendix G reports results for variants of training in which we used image augmentations and hard distractors.

3.3 Datasets

As nearly all agents rely on vision modules pre-trained on the ILSVRC2012 training set, we sample images from the validation data of that same dataset (50,000 images) to teach them to play the referential game, while reserving 10% of those images for testing (note that we do not use image annotations). Thus, our *ImageNet1k* communication training and testing sets are both extracted from the original ILSVRC2012 *validation* set.

Agents are also tested on an out-of-domain (*OOD*) dataset containing classes from the larger ImageNet-21k repository, as pre-processed by Ridnik et al. (2021). We selected the new classes among those that are neither hypernyms nor hyponyms of ImageNet1k classes, and we made sure that no OOD class had a WordNet path similarity score[2] above 0.125 with any ImageNet1k class.[3] We moreover used a number of heuristics, combined with manual inspection, to make sure the new classes were more or less at the same level of granularity as the ImageNet1k categories. After applying these filters, we were left with 52 classes denoting objects that belong to semantic domains disjoint from those represented in ImageNet1k, such as trees (*olive tree*, *fir*, *red pine*) and human professions (*carpenter*, *physician*, *organ grinder*). For each of them, we sampled all images available in the pre-processed ImageNet-21k dataset of Ridnik et al. (2021) (guaranteed to be at least 450). We used 90% of the OOD data for testing OOD communication accuracy (Section 4.2 below) and to train the classifiers in the experiments reported in Appendix H. The remaining 10% was used to test the latter classifiers.[4]

We further test the agents that were communication-trained on ImageNet1k on 3 different datasets, two of which have very different image types from those present in ImageNet, namely: 1) Cifar100 (Krizhevsky et al., 2009), which, like ImageNet1k, is made of images that tend to foreground a single object; 2) Places205 (Zhou et al., 2014), focusing on scenery rather than objects; 3) CelebA: (Liu et al., 2015), whose images depict face close-ups.

[1] `https://github.com/facebookresearch/EGG`, scripts from our experiments are in ./egg/zoo/pop

[2] As implemented in the NLTK toolkit: `https://www.nltk.org/`.

[3] The COCO dataset, used to pre-train one of our visual modules, contains four labels slightly above the threshold, with maximum similarity at 0.17.

[4] We provide scripts to reproduce our ImageNet1k and OOD datasets at `https://github.com/mahautm/emecom_pop_data`

	Accuracy (16)	Learning Time (16)	Accuracy (64)	Learning Time (64)
Homogeneous	99.3 ± 0.8	9 ± 8	98.6 ± 2.9	6.5 ± 8.1
Heterogeneous	95.3 ± 3.4	7 ± 3	99.2 ± 1.1	9.7 ± 6.5
Population	96.8 ± 2.7	28	98.2 ± 2.2	24

Table 2: Percentage *accuracy* and *learning time* of agents playing the referential game. Learning time counts the number of epochs until maximum accuracy is reached (bigger numbers indicate slower convergence). Results are reported for two message dimensions. The *homogeneous* row reports mean scores and standard deviations across 7 pairs of same-architecture nets, each trained separately. The scores in the *heterogeneous* row are averaged across all 42 possible different-architecture pairings, each trained separately. Population accuracy is averaged across all 49 possible net pairings after joint training. There is no standard deviation around population learning time as we have a single jointly-trained population.

4 Experiments

We first compare single agent pairs and larger communities in the straightforward setup in which test images depict new instances of referents used for communication training (Section 4.1). We then look at protocol generalization along two axes: communicating about new *referents* (Section 4.2) and communicating with new *agents* (Section 4.3).

4.1 Referential communication of homogeneous and heterogeneous networks

Starting from the baseline scenario in which there are only one sender and one receiver with identical visual modules (one-to-one *homogeneous* setting), we look at the effect of pairing two *heterogeneous* architectures (one-to-one *heterogeneous* setting), and then scale up to training a full population of agents at once (*population* setting).

The results are presented in Table 2. We observe first that it is possible to quickly train two homogeneous agents to near perfect referential accuracy (first row). Importantly, as shown in the second row of the table, **pairing agents with different visual architectures only weakly affects accuracy and learning time, if at all**. We conjecture that this ease of training in the heterogeneous setup is at least partially due to the fact that different architectures must ultimately extract comparable semantic features from images during pre-training, facilitating the task of making them communicate (although, as we will see below, there is no strong correlation between similarity of pre-trained visual module representations and communication performance). Detailed performance across all tested agent pairs is available in Appendix I, and we comment on some general patterns observed there in what follows. We focus here on agents trained with 16-dimensional messages, as with the 64-dimensional channel we are uniformly near the ceiling.

Communication is easy for pairs that have different architectures. For example, communication between a ViT sender and a VGG receiver reaches 95% accuracy in 4 epochs. Communication is also easy for visual modules based on different training objectives: for example, ResNet-to-DINO communication reaches 98% accuracy in 12 epochs. It might look like communication is harder for pairs trained on different corpora, as 4/5 pairs requiring 10 or more epochs to train involve ResNet-COCO as the receiver agent. However, the latter also requires 29 epochs to converge in the homogeneous setup, suggesting that the (relative) issue with this module is the mismatch between its pre-training corpus (COCO) and the one used for communication training (ImageNet1k), rather than its heterogeneity with respect to the other agents.[5]

It is also possible to train the full agent population to very high accuracy in relatively few epochs (*Population* row in Table 2). In this setup, we use all 7 modules as both senders and receivers, randomly pairing them at training time, ensuring each agent interacts with every other agent. A common communication protocol emerges that is mutually intelligible across all 49 agent pairings. Note that the large increase in learning time compared to the one-to-one setups is only apparent, because during population

[5]The somewhat larger average learning time and corresponding standard deviation in the homogeneous 16-dimensional setup compared to the heterogeneous one are accounted for by the extra time it takes to train the ResNet-COCO sender-receiver pair. Note that, during heterogeneous training, at least one of the two agents is always ImageNet-based.

16-dimensional	Single-class	OOD
Homogeneous	47.2 ± 3.4	94.8 ± 10.4
Heterogeneous	31.0 ± 22.2	82.2 ± 13.8
Population	34.7 ± 6.8	72.2 ± 44.8

Table 3: Percentage accuracy on ImageNet Out of Domain sets for 16-dimensional messages.

64-dimensional	Single-class	OOD
Homogeneous	47.4 ± 6.4	90.5 ± 8.0
Heterogeneous	48.6 ± 2.1	62.9± 17.6
Population	36.5 ± 8.6	72.2 ± 13.8

Table 4: Percentage accuracy on ImageNet Single-class and Out of Domain sets for 64-dimensional messages

training each agent is only seeing 1/7 of the data in each epoch.[6] Thus, in terms of actual data exposure, a joint count of 28 (or 24 when using the 64-dimensional channel) epochs correspond to 4 (3.3) effective epochs of data exposure for a single agent, on average. Convergence is thus faster on average in population training than in one-to-one training.

We investigated whether the (generally small) differences in accuracy or learning time between agents with different visual modules is accounted for by the underlying discrepancy between their pre-trained visual representations. As different visual modules have different output dimension, we used RSA (Kriegeskorte et al., 2008) to measure the correlation between visual module output similarity and accuracy/learning time in communication training (measured for population pairs and one-to-one couplings, respectively). We did not find a significant correlation in either case, suggesting that communication training is quite robust to underlying visual representation differences.

4.2 Referential generalization

Having established with the previous experiment that it is possible to train a light communication layer that allows networks with heterogeneous architectures to successfully agree on a target referent, we go back to the questions about referent generalization we asked in the introduction. First, we explore whether the protocol can make more granular distinctions among objects coming from the same ImageNet1k classes that were used to develop it. For these purposes, we built a special test set where *all* distractors are from the same ImageNet1k class as the target (so that, say, one target magpie needs to be distinguished from other magpies, instead of swans and bullfrogs). We tested all 1,000 ImageNet1k classes in smaller batches of 32 candidates, to ensure we had enough images in all cases. In this *single-class* setup, random baseline accuracy is at around 3.1%. Note that, since we are interested in out-of-the-box zero-shot generalization, we use the very same protocols induced with random distractors in the experiments above, without any special adaptation to the single-class setup.

Tables 3 and 4 show that **communication is at least partially successful at a more granular level than ImageNet1k classes**, despite a large drop from the random-distractor performance reported above. There is a noticeable discrepancy between 16 (Table 3) and 64-dimensional messages (Table 4), with the latter being generally better than the former, especially in the heterogeneous setup. We find this result intriguing, as we would have expected smaller message dimensionality to act as a regularizing bottleneck, leading to better generalization performance.

Next, we ask whether a communication protocol can also generalize, zero-shot, to referents that were not seen at training time. In particular, the systems trained on the referential game using ImageNet1k data are now tested on the OOD dataset, that is entirely composed of new-class objects (see Section 3.3 above).

[6]In other words, Table 2 is comparing on the same scale the time it takes to train 2 agents in the one-to-one setups to the time it takes to train 14 agents in the population setup. The difference is even sharper if we consider specific *pairs* of population agents, as at each turn an agent is paired with one of seven distinct partners. In Appendix J, we show that, if we train the population for 7 times more epochs, so that each population agent sees as much data as an agent in the one-to-one settings, population accuracy further slowly increases, although it still generally lags behind that of one-to-one training.

	Cifar100	**Places205**	**CelebA**
Homogeneous	80.5 ± 17.7	100 ± 0.0	98.1 ± 2.0
Heterogeneous	25.8 ± 15.7	94.7 ± 6.4	48.1 ± 20.1
Population	27.8 ± 44.8	85.2 ± 35.5	38.3 ± 48.6

Table 5: Percentage accuracy on unseen datasets (Cifar100, Places205 and CelebA) for 64-dimensional messages.

As Tables 3 and 4 show, compared to in-domain results (Table 2), there is a significant accuracy drop (larger in the more challenging heterogeneous and population setups), but performance remains good enough to suggest that **the protocol is able to generalize to images depicting referents not seen during training well above chance level** (recall that chance performance is here at $1/64 \approx 1.6\%$). Larger dimensionality seems again to help generalization, at least in the homogeneous and heterogeneous setups.

Finally, we consider a different kind of referent generalization, in which we take the agents that were communication-trained on ImageNet, and test them on other datasets, that might contain very different referent distributions. In particular, Cifar100 focuses on a small number of concepts at a higher level of granularity than ImageNet;[7] Places205 focuses on scenes rather than objects; CelebA is entirely composed of celebrity faces.

Table 5 shows that 64-dimensional communication is still possible in this zero-shot dataset-transfer experiment (see Appendix K for the 16-dimensional case). With chance performance still at $1/64 \approx 1.6\%$, with Places205 we observe even higher accuracy than with the ImageNet OOD set. As shown in the examples of Fig. 3 and in Appendix P, Fig. 16, this might be at least partially explained by the presence of familiar objects in the scenes depicted in this dataset. Performance on the CelebA dataset is near-perfect for homogeneous agents, and comparable to that obtained on the single-class set for the other agents. This makes sense, as this face-only dataset can be seen as an extreme case of the single-class setup. We conjecture that heterogeneous population pairs are less likely to converge on low-level features that might help catching the more granular differences of the single-class datasets. Finally, it is surprising that, while still much higher than random, performance is lowest on Cifar100, which is, like ImageNet, an object-centric dataset. By inspecting the Cifar100 images, we realized that they have a much lower resolution than those of ImageNet, looking much blurrier. As we will see below in Section 4.4.3, the communication protocol is not robust to image blurring.

Results for 16-dimensional communication are presented in Appendix K. They follow a similar pattern but with lower accuracies, especially in the homogeneous pair setup. We observe that the extra dimensions have a low impact on in-domain performance (+ 2% for all three agent pairing setups), but are very useful for referent generalization in all cases, reaching a maximum of + 75% for homogeneous pairs in Places205.

Overall, the main takeaways from the referent generalization experiments are the following. First, out-of-domain communication works out of the box with results way above chance, although there is a drop with respect to in-domain communication. Second, generalization is more successful when generalizing to new objects and scenes than when the agents must distinguish between objects of the same class

4.3 Agent generalization

Having tested how well the protocol can be applied to new *referents*, we now consider whether it is possible to efficiently extend it to new *agents*, as in the practical scenario where a new autonomous device is added to an existing network of such items. In particular, we ask whether a new agent joining a community of agents already trained to communicate with each other can efficiently learn their communication protocol.

[7]Note that, while the agents are trained on ImageNet1K data, Cifar100 was used for the limited hyperparameter searches we describe in Appendix D.

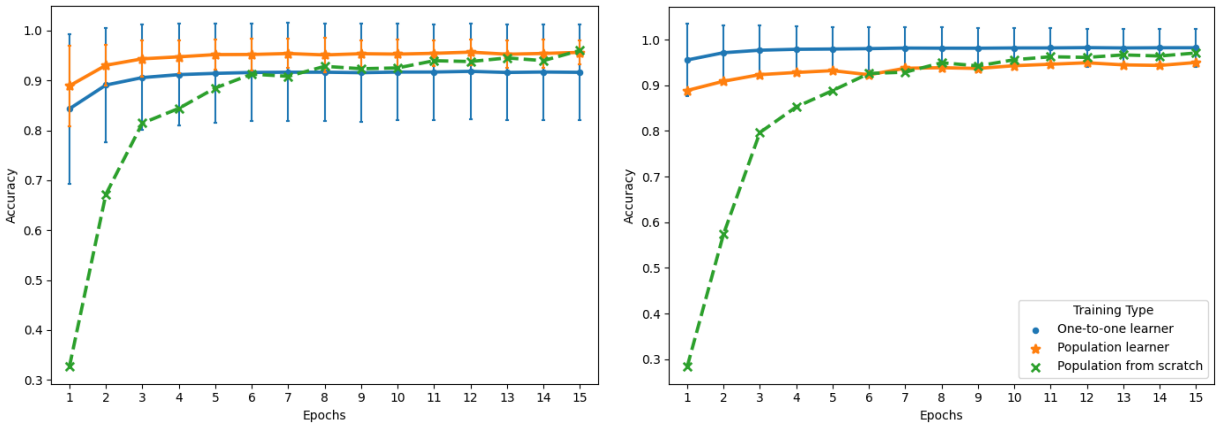

Figure 2: Test accuracy and learning speed of learner agents (left: 16-dimensional messages; right: 64-dimensional messages). Blue line: learning curve on test data for learner agent added to a communicating pair, averaged across all possible heterogeneous triples. Orange line: learning curve for a learner agent added to an existing community, averaged across all possible leave-one-out cases. Vertical bars indicate standard deviation across cases. As a baseline for learning speed, the dashed green line shows the learning curve when training the whole 7x7 population at once from scratch.

To test ease of learning of a communication protocol, we add a single network, which we call the *learner* agent, to an existing community, either as sender or as receiver.[8] This new agent has to play the referential game with the original agents and learn their protocol. To single out ease of learning of the communication protocol itself, and not the original agents' adaptability, we freeze all communication layer parameters except for the learner agent's. The new communication layer is therefore the only one being updated. The focus of this experiment is on the heterogeneous learners, where the new agent's vision module is different from that of the original agents. We nonetheless observe that, in the homogeneous case (not reported here), communication protocols are learned very quickly, needing at most one epoch to reach perfect or near-perfect accuracy.

In the (heterogeneous) one-to-one setup, we train a communication protocol for each of the 49 possible different architecture pairs.[9] For each pair, we then add a learner sender or receiver for every vision module not in the original pair (e.g., if the protocol was trained on the ResNet152-Swin pair, we test, as both learner senders and receivers, Inception, VGG 11, ViT-B/16, ViT-S/16-DINO and Resnet50-COCO). In the population setup, the 7 possible leave-one-out populations of 6 different senders and 6 different receivers are trained on the referential game, and, for each, the learner agent will use the 7th vision module that was left out, acting as either sender or as receiver.

Test accuracy and learning speed of the learner agents are reported in Fig. 2. In all runs with a 64-dimensional communication channel, **the learner agent succeeds at learning the communication protocol** with accuracy of at least 90%. There is some more variance with 16-dimensional messages, but in this case as well nearly all runs converge to very high accuracy. Receivers learn better and faster on average (94%/95% for one-to-one with 16/64-messages, respectively, and 96%/97% for population) than senders (88%/95% and 95%/97%, respectively). We don't have an explanation for this, but we believe it is related to the fact that senders must perform more exploration when associating the target image to a message in the emergent protocol, whereas the role of the receivers is more deterministic, in that they must just decode the sender messages (see Rita et al., 2020, for sender/receiver learning asymmetries in emergent communication).

The comparison between the one-to-one and population setups reveals no clear winner: population accuracy is on average higher than one-to-one accuracy with 16-dimensional messages but lower with 64-dimensional

[8]Alternatively, a single pair of agents could initially be trained, and then all other agents could be sequentially added to the growing community. Appendix L shows that the all-at-once approach we report here outperforms sequential population training.

[9]These pairs also include homogeneous senders and receivers, but we will always add an heterogeneous agent to the pair.

messages. Population accuracy, however, is more stable in both setups, showing very little variance from case to case.

Regarding learning speed, **agents that learn a pre-existing communication protocol reach high accuracy faster than it would take to retrain the whole population from scratch**, as illustrated by the population-from-scratch baseline in Fig. 2. The communication protocol is indeed initially very easy to learn for a new agent. There is no clear difference in learning speed between the one-to-one and population setups.

We further replicate the agent generalization experiments with other pre-trained models that had not been used at any point during our experiments so far: LeViT: Graham et al. (2021), CaiT: Touvron et al. (2021), ResNeXt: Xie et al. (2017), DenseNet: Huang et al. (2017). Accuracies are above 95% from the first epoch for all settings (see Appendix M), strongly confirming the generality of the protocol, and suggesting that, once the latter has been developed, it can easily be transferred to novel architectures.

We also experiment with a visual module that has been trained with a natural-language-mapping objective (CLIP Radford et al. (2021)), since this might have introduced biases that makes it very different from purely visual models. We find that this is not the case. No drop in performance is observed for generalization of CLIP-induced protocols to new agents, or to new data: adaptation to this potentially outlying representation is not slower or less efficient (see Appendix N).

4.4 Protocol analysis

Having shown its effectiveness, we turn now to a qualitative and quantitative examination of the emergent protocol. For this analysis, we focus on the overall better-performing 64-dimensional message setup.

4.4.1 Probing for degenerate communication

We begin by applying the "Gaussian blobs" sanity test introduced by Bouchacourt & Baroni (2018). We check whether the agents trained to communicate on the ImageNet1k dataset are able, at test time, to play the referential game on blobs of Gaussian noise instead of genuine images. Success would mean the agents developed degenerate communication strategies, focusing on pixel-level image features that can transfer to the task of discriminating between blobs of Gaussian noise, rather than on more desirable high-level semantic information. We find that all one-to-one and population-trained pairs are indeed at chance level on Gaussian blobs, suggesting they are not just communicating about low-level image features.

4.4.2 Disentangling meaning with a Sparse Autoencoder

To investigate which high-level features are used in communication, we use dictionary learning, which has proven useful to identify interpretable features in multimodal models (Parekh et al., 2024), and more specifically Sparse AutoEncoders (SAEs) (Bricken et al., 2023; Cunningham et al., 2023; Rajamanoharan et al., 2024; Templeton et al., 2024). In our case, the SAE consists of single-layer encoders and decoders, with an added ReLu nonlinearity for the encoder. The encoder projects 64-dimensional messages to an expanded hidden space (we use a hidden space of $16 \times 64 = 1024$ dimensions). Training is done with a mean-square error reconstruction loss, and an L1 regularization loss to add sparsity (weight of the L1 term is set to 0.01). The sparsity component of the loss encourages storing meaningful information in individual dimensions. We train the SAE using messages corresponding to images from the communication training set (ImageNet1k, see section 3.3). Informally varying the SAE hyperparameters did not impact our general conclusions. We present SAE results for messages from a VGG 11 sender + ViT-B/16 receiver pair, which are representative of other cases.

First and most importantly, we observe that the dimensions uncovered by the SAE correspond to understandable semantic features. In particular, we qualitatively assess this by looking, for each SAE dimension, at the images corresponding to the messages closest to that dimension.[10] We observe that images clustered around a dimension share a common human-interpretable meaning. In Fig. 3, which contains the images

[10]We were able to do this for all 1024 dimensions because many of them share the same neighbors.

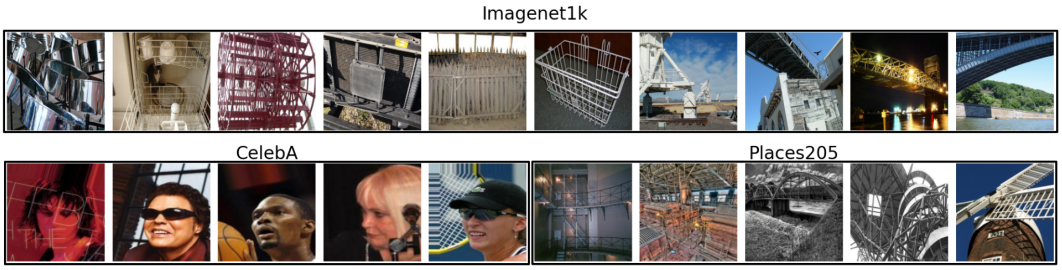

Figure 3: **Top**: ImageNet1k images which have messages closest to a chosen one-hot vector in SAE space. **Bottom Left**: CelebA images with messages closest to the same sparse dimension. **Bottom right**: 5 closest Places205 Images. No image from CelebA and Places205 is seen at training time by either sender, receiver or SAE.

closest to a representative SAE feature, we see different metallic grids. It is worth noting that they do not all share the same ImageNet1k class. The messages clustering around the same SAE vectors are abstract enough to overcome perceptual variation, with for example one of the images in Fig. 3 being photographed in night-time conditions (penultimate, first row), while the others all have good lighting conditions. We present additional representative examples in Appendix O (Fig. 11). Additional evidence for the semantic nature of the messages is provided in a qualitative error analysis in Appendix P.

SAE features also inform us about referent generalization. We use the same sender and SAE trained on ImageNet1k to extract the k-nearest messages from the OOD datasets to each one-hot SAE vector. In general, the closest OOD messages to each SAE vector also form human-interpretable clusters, noisily sharing properties with the corresponding ImageNet1k training images. In the case of Places205, bottom right in Fig. 3, the images considered all contain an object with a metallic grid. For the more strongly OOD CelebA dataset, bottom left, pictures of celebrities tend to show either parallel lines, or in one case a metallic object. In general, OOD messages are futher away from one-hot SAE features than in-domain messages are, reflecting the fact that the corresponding images less closely match the properties captured by the features.[11]

From another perspective, instead of looking at which OOD messages are nearer pre-selected SAE vectors, we can ask which SAE vectors are closer to any message from an OOD dataset. Messages describing OOD images cluster around SAE vectors with properties relevant to the dataset. The CelebA messages tend to be closer to the SAE dimensions representing people, while Places205 messages are closer to SAE vectors corresponding to urban settings, or landscapes.[12] We provide an example of each in Fig. 12 of Appendix O.

4.4.3 Perturbation analysis

In a next set of analyses, we gain insight on the information encoded in the message by looking at how image perturbations affect communication (an analysis of direct perturbation of the communication channel itself is reported in Appendix Q). The way in which performance degrades in response to different perturbations should be informative about the image features that the communication protocol is relying on, and whether they are aligned with features that are intuitively crucial for our own high-level characterization of images. These experiments can also be seen as a further way to perform out-of-domain testing, where a protocol that was trained on non-augmented data is evaluated on perturbed images at test time.

The effects of the perturbations on an example image are shown on the right in Fig. 4. We perturb images from the ImageNet1k dataset that were seen by the agents during referential game training, where the receivers have perfect accuracy. In each experiment, we apply the same transformation to all images, both

[11]On average, there are 56 ImageNet1k messages closer to a feature than the closest CelebA message. For Places205, which is less OOD, there are on average 7 ImageNet1K messages closer to a feature.

[12]To avoid pareidolia, we verified this claim in a small experiment. We prepared 30 sets of 10 ImageNet1k images, corresponding either to a feature close to Places205 images, or to one feature corresponding to CelebA images, or to neither. One of the authors then labeled them, without knowing their source, for whether they contained foregrounded faces (close to CelebA), depicted landscapes or urban settings (close to Places205), or neither. Performance was well above random chance.

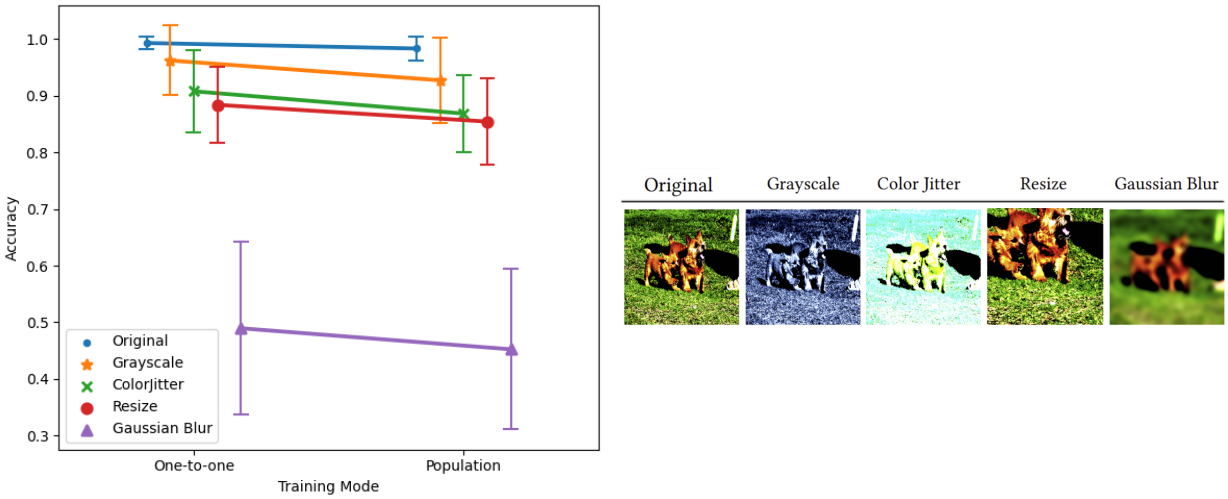

Figure 4: Accuracy after various image perturbations for the one-to-one and population setups (left). Gaussian blur was uniformly sampled within the [0.1,10] range. Mean accuracies and corresponding standard deviations are given across all 36 possible agent pairs. We add a small horizontal offset to the accuracy values for different perturbations to make them all visible. The horizontal lines connecting one-to-one and population accuracies for the same perturbation are meant to ease comparison between the two settings. Random baseline is 1.6% (randomly selecting one of the 64 images). Perturbation examples are provided on the right.

those seen by the sender and those seen by the receiver. Note that we test senders and receivers that have been trained with non-corrupted images, and only face the perturbations at test time.

Results for both the one-to-one and the population setups are reported in Fig. 4 (left). All ablations affect accuracy. However, the color ablations (transforming the image to *grayscale* and *jittering colors*) and *resizing* the image are having a much smaller impact on performance than adding *Gaussian blur*. This is in line with our intuition about how much these changes should affect the ability to decode the contents of an image. As the examples on the right in Fig. 4 show, color and size ablations don't normally affect the human ability to discriminate the object depicted in the image, whereas blurring the image can easily make its contents difficult to decode for us as well.

We finally observe that all perturbation types affect one-to-one and population-trained agents in a similar manner, with population-trained agents being marginally more affected.[13]

4.4.4 Specificity of population protocol

An important distinction in favor of population-based training is that in this setup, as shown in Fig. 5, the senders converge to using very similar messages to denote the same image, approximating a single protocol. Note that the observation is not trivial: different senders could in principle have developed distinct protocols, with the receivers learning to process the union of these distinct protocols (we informally observed something of the sort taking place in the emergence of discrete population-based communication). Fig. 5 also shows that the distance between one-to-one senders, that have been trained independently of one another, is significantly larger on average than that between population-trained senders, and virtually indistinguishable from the baseline of averaging distances between messages representing different images for a single sender.

To further illustrate, and build upon, the observation that population training has converged to a single protocol, in Appendix H we report an experiment in which the common representations induced in this setting are used for zero-shot classifier transfer.

[13]If we continue training the population as we do in Appendix J, the gap between population-trained and one-to-one agents eventually disappears.

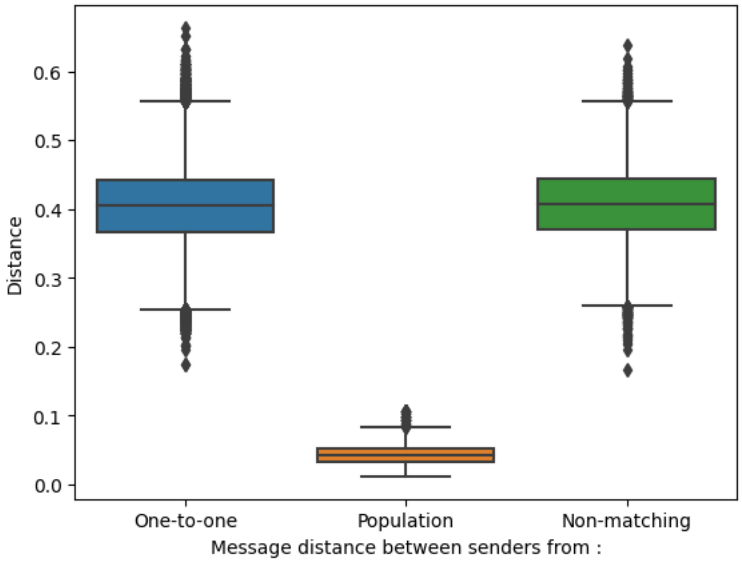

Figure 5: Distributions of cosine distances between messages sent by two different senders for the same ImageNet1k training set images. The different senders are either trained in the heterogeneous one-to-one setup (blue) or in the same population (orange). As a baseline, the green boxplot shows distances between the messages produced for *different* input images by population-trained VGG 11 and ViT-B/16 senders.

5 Conclusion

Coming back to the questions we asked in the Introduction, we found that it is possible for agents based on pre-trained deep visual modules with different architectures, training objectives and training data to induce a successful referential communication protocol through a self-supervised training procedure that only involves a light communication layer, without touching the visual module weights. The architectural extensions are simple and straightforward, suggesting that differing underlying pre-trained visual models already converged to similar representations.

The networks can use the emergent protocol to communicate about referents that are only distinguishable at a more granular level than used during communication training; and they can communicate about referents coming from categories or even datasets that were not seen during pre-training nor in the communication protocol induction phase.

Importantly, we showed that a new deep net agent can successfully learn the protocol developed by an existing community, and that it can do so in less time than it would take to re-train the enlarged community including the new agent from scratch. This points to the possibility of developing a "universal" deep net protocol, that could be quickly taught to any new model before it is deployed in multi-network communication scenarios. We further found that the emergent protocol possesses a number of intuitive characteristics suggesting that it is focusing on semantic properties of the objects depicted in images, rather than on low-level visual features.

Despite our encouraging set of initial results, clearly much work is still needed before the envisaged communication layer can be of practical use. First, we observed a drop in performance in the referent generalization experiments compared to communication about in-domain referents. Future work should further explore the generality of the protocol, and devise ways to broaden it.

We have motivated our study in terms of nets embedded in robots and self-driving cars. Such systems will not perceive the world as a discrete set of pictures, but rather as a fully embodied egocentric image flow. This scenario obviously poses further challenges. For example, two agents that need to communicate about an object would almost never have an identical view of it. Scaling up our approach to this setup is another important direction for future work.

Referent denotation is an important building block of communication, but it's clearly just the starting point, and further work should extend deep net communication to other functions of language, such as highlighting different properties of objects, describing actions, and distinguishing between providing information, asking for it and giving instructions. These features will in turn require extending the setup to multiple exchanges, and to agents that can function both as senders and as receivers.

Acknowledgments

We thank Agnieszka Słowik for early contributions to this work. We are also grateful to Thomas Brochhagen, Dan Dediu, Rahma Chaabouni, Emily Cheng, Valentino Maiorca, Luca Moschella, Clément Moulin Frier, the members of the COLT group and the TMLR editor and reviewers for useful feedback. This project has received funding from the European Research Council (ERC) under the European Union's Horizon 2020 research and innovation programme (grant agreement No. 101019291). We also received funding from the Catalan government (AGAUR grant SGR 2021 00470). This paper reflects the authors' view only, and the funding agencies are not responsible for any use that may be made of the information it contains.

References

Yamini Bansal, Preetum Nakkiran, and Boaz Barak. Revisiting model stitching to compare neural representations. In *Proceedings of NeurIPS*, pp. 225–236, Online, 2021.

Diane Bouchacourt and Marco Baroni. How agents see things: On visual representations in an emergent language game. In *Proceedings of EMNLP*, pp. 981–985, Brussels, Belgium, 2018.

Trenton Bricken, Adly Templeton, Joshua Batson, Brian Chen, Adam Jermyn, Tom Conerly, Nick Turner, Cem Anil, Carson Denison, Amanda Askell, Robert Lasenby, Yifan Wu, Shauna Kravec, Nicholas Schiefer, Tim Maxwell, Nicholas Joseph, Zac Hatfield-Dodds, Alex Tamkin, Karina Nguyen, Brayden McLean, Josiah E Burke, Tristan Hume, Shan Carter, Tom Henighan, and Christopher Olah. Towards monosemanticity: Decomposing language models with dictionary learning. *Transformer Circuits Thread*, 2023. https://transformer-circuits.pub/2023/monosemantic-features/index.html.

Rodrigo Canaan, Julian Togelius, Andy Nealen, and Stefan Menzel. Diverse agents for ad-hoc cooperation in Hanabi. In *Proceedings of CoG*, pp. 504–511, London, UK, 2019.

Angelo Cangelosi and Domenico Parisi (eds.). *Simulating the evolution of language*. Springer, New York, 2002.

Boaz Carmeli, Ron Meir, and Yonatan Belinkov. Emergent quantized communication. *CoRR*, abs/2211.02412, 2022. doi: 10.48550/arXiv.2211.02412. URL `https://doi.org/10.48550/arXiv.2211.02412`.

Mathilde Caron, Hugo Touvron, Ishan Misra, Hervé Jégou, Julien Mairal, Piotr Bojanowski, and Armand Joulin. Emerging properties in self-supervised vision transformers. In *Proceedings of ICCV*, pp. 9650–9660, Online, 2021.

Rahma Chaabouni, Florian Strub, Florent Altché, Eugene Tarassov, Corentin Tallec, Elnaz Davoodi, Kory Wallace Mathewson, Olivier Tieleman, Angeliki Lazaridou, and Bilal Piot. Emergent communication at scale. In *Proceedings of ICLR*, Online, 2022. Published online: `https://openreview.net/group?id=ICLR.cc/2022/Conference`.

Ting Chen, Simon Kornblith, Mohammad Norouzi, and Geoffrey Hinton. A simple framework for contrastive learning of visual representations. In Hal Daumé III and Aarti Singh (eds.), *Proceedings of the 37th International Conference on Machine Learning*, volume 119 of *Proceedings of Machine Learning Research*, pp. 1597–1607. PMLR, 13–18 Jul 2020. URL `https://proceedings.mlr.press/v119/chen20j.html`.

Xinlei Chen, Hao Fang, Tsung-Yi Lin, Ramakrishna Vedantam, Saurabh Gupta, Piotr Dollár, and C. Lawrence Zitnick. Microsoft COCO captions: Data collection and evaluation server. *CoRR*, abs/1504.00325, 2015.

Morten Christiansen and Simon Kirby (eds.). *Language Evolution*. Oxford University Press, Oxford, UK, 2003.

Michael Cogswell, Jiasen Lu, Stefan Lee, Devi Parikh, and Dhruv Batra. Emergence of compositional language with deep generational transmission. `https://arxiv.org/abs/1904.09067`, 2019.

Hoagy Cunningham, Aidan Ewart, Logan Riggs, Robert Huben, and Lee Sharkey. Sparse autoencoders find highly interpretable features in language models. *arXiv preprint arXiv:2309.08600*, 2023.

Kasra Darvish, Edward Raff, Francis Ferraro, and Cynthia Matuszek. Multimodal language learning for object retrieval in low data regimes in the face of missing modalities. *Transactions on Machine Learning Research*, 2023. Published online: `https://openreview.net/forum?id=cXa6Xdm0v7`.

Karan Desai and Justin Johnson. VirTex: Learning Visual Representations from Textual Annotations. In *CVPR*, 2021.

Roberto Dessì, Eugene Kharitonov, and Marco Baroni. Interpretable agent communication from scratch (with a generic visual processor emerging on the side). In *Proceedings of NeurIPS*, Online, 2021. Published online: `https://papers.nips.cc/paper/2021`.

Alexey Dosovitskiy, Lucas Beyer, Alexander Kolesnikov, Dirk Weissenborn, Xiaohua Zhai, Thomas Unterthiner, Mostafa Dehghani, Matthias Minderer, Georg Heigold, Sylvain Gelly, Jakob Uszkoreit, and Neil Houlsby. An image is worth 16x16 words: Transformers for image recognition at scale. In *International Conference on Learning Representations*, 2021. URL `https://openreview.net/forum?id=YicbFdNTTy`.

Alaaeldin El-Nouby, Natalia Neverova, Ivan Laptev, and Hervé Jégou. Training vision transformers for image retrieval. `http://arxiv.org/abs/2102.05644`, 2021.

Jakob Foerster, Ioannis Alexandros Assael, Nando de Freitas, and Shimon Whiteson. Learning to communicate with deep multi-agent reinforcement learning. In *Proceedings of NIPS*, pp. 2137–2145, Barcelona, Spain, 2016.

Vincent Francois-Lavet, Peter Henderson, Riashat Islam, Marc Bellemare, and Joelle Pineau. An introduction to deep reinforcement learning. *Foundations and Trends in Machine Learning*, 25(3-4):1–140, 2018.

Kent Gauen, Ryan Dailey, John Laiman, Yuxiang Zi, Nirmal Asokan, Yung-Hsiang Lu, George K. Thiruvathukal, Mei-Ling Shyu, and Shu-Ching Chen. Comparison of visual datasets for machine learning. In *2017 IEEE International Conference on Information Reuse and Integration (IRI)*, pp. 346–355, 2017. doi: 10.1109/IRI.2017.59.

Rohit Girdhar, Alaaeldin El-Nouby, Zhuang Liu, Mannat Singh, Kalyan Vasudev Alwala, Armand Joulin, and Ishan Misra. ImageBind: One embedding space to bind them all. In *Proceedings of CVPR*, pp. 15180–15190, Vancouver, Canada, 2023.

Laura Graesser, Kyunghyun Cho, and Douwe Kiela. Emergent linguistic phenomena in multi-agent communication games. In *Proceedings of EMNLP*, pp. 3700–3710, Hong Kong, China, 2019.

Benjamin Graham, Alaaeldin El-Nouby, Hugo Touvron, Pierre Stock, Armand Joulin, Herve Jegou, and Matthijs Douze. Levit: A vision transformer in convnet's clothing for faster inference. In *Proceedings of the IEEE/CVF International Conference on Computer Vision (ICCV)*, pp. 12259–12269, October 2021.

Jean-Bastien Grill, Florian Strub, Florent Altché, Corentin Tallec, Pierre Richemond, Elena Buchatskaya, Carl Doersch, Bernardo Avila Pires, Zhaohan Guo, Mohammad Gheshlaghi Azar, Bilal Piot, Koray Kavukcuoglu, Remi Munos, and Michal Valko. Bootstrap your own latent - a new approach

to self-supervised learning. In H. Larochelle, M. Ranzato, R. Hadsell, M.F. Balcan, and H. Lin (eds.), *Advances in Neural Information Processing Systems*, volume 33, pp. 21271–21284. Curran Associates, Inc., 2020. URL https://proceedings.neurips.cc/paper_files/paper/2020/file/f3ada80d5c4ee70142b17b8192b2958e-Paper.pdf.

Serhii Havrylov and Ivan Titov. Emergence of language with multi-agent games: Learning to communicate with sequences of symbols. In *Proceedings of NIPS*, pp. 2149–2159, Long Beach, CA, 2017.

Kaiming He, Xiangyu Zhang, Shaoqing Ren, and Jian Sun. Deep residual learning for image recognition. In *Proceedings of CVPR*, pp. 770–778, Las Vegas, NV, 2016.

Sepp Hochreiter and Jürgen Schmidhuber. Long short-term memory. *Neural Computation*, 9(8):1735–1780, 1997.

Gao Huang, Zhuang Liu, Laurens Van Der Maaten, and Kilian Q Weinberger. Densely connected convolutional networks. In *Proceedings of the IEEE conference on computer vision and pattern recognition*, pp. 4700–4708, 2017.

Minyoung Huh, Brian Cheung, Tongzhou Wang, and Phillip Isola. The Platonic representation hypothesis. In *Proceedings of ICML*, pp. 20617–20642, Vienna, Austria, 2024.

Eric Jang, Shixiang Gu, and Ben Poole. Categorical reparameterization with Gumbel-Softmax. In *Proceedings of ICLR Conference Track*, Toulon, France, 2017. Published online: https://openreview.net/group?id=ICLR.cc/2017/conference.

Eugene Kharitonov, Rahma Chaabouni, Diane Bouchacourt, and Marco Baroni. EGG: a toolkit for research on emergence of language in games. In *Proceedings of EMNLP (System Demonstrations)*, pp. 55–60, Hong Kong, China, 2019.

Daewoo Kim, Sangwoo Moon, David Hostallero, Wan Ju Kang, Taeyoung Lee, Kyunghwan Son, and Yung Yi. Learning to schedule communication in multi-agent reinforcement learning. In *Proceedings of ICLR*, New Orleans, LA, 2019. Published online: https://openreview.net/group?id=ICLR.cc/2019/conference.

Nikolaus Kriegeskorte, Marieke Mur, and Peter Bandettini. Representational similarity analysis: Connecting the branches of systems neuroscience. *Frontiers in Systems Neuroscience*, 2(4):1–28, 2008.

Alex Krizhevsky, Vinod Nair, and Geoffrey Hinton. Cifar-100 (canadian institute for advanced research), 2009. URL http://www.cs.toronto.edu/~kriz/cifar.html.

Samuel Lavoie, Christos Tsirigotis, Max Schwarzer, Ankit Vani, Michael Noukhovitch, Kenji Kawaguchi, and Aaron C. Courville. Simplicial embeddings in self-supervised learning and downstream classification. In *ICLR*. OpenReview.net, 2023.

Angeliki Lazaridou and Marco Baroni. Emergent multi-agent communication in the deep learning era. https://arxiv.org/abs/2006.02419, 2020.

Angeliki Lazaridou, Alexander Peysakhovich, and Marco Baroni. Multi-agent cooperation and the emergence of (natural) language. In *Proceedings of ICLR Conference Track*, Toulon, France, 2017. Published online: https://openreview.net/group?id=ICLR.cc/2017/conference.

Karel Lenc and Andrea Vedaldi. Understanding image representations by measuring their equivariance and equivalence. *International Journal of Computer Vision*, 127(5):456–476, 2019.

Fushan Li and Michael Bowling. Ease-of-teaching and language structure from emergent communication. In *Proceedings of NeurIPS*, Vancouver, Canada, 2019. Published online: https://papers.nips.cc/paper/2019.

Yixuan Li, Jason Yosinski, Jeff Clune, Hod Lipson, and John Hopcroft. Convergent learning: Do different neural networks learn the same representations? In *Proceedings of ICLR Conference Track*, San Juan, Puerto Rico, 2016. Published online: http://www.iclr.cc/doku.php?id=iclr2016:main.

Paul Pu Liang, Yiwei Lyu, Xiang Fan, Jeffrey Tsaw, Yudong Liu, Shentong Mo, Dani Yogatama, Louis-Philippe Morency, and Russ Salakhutdinov. High-modality multimodal transformer: Quantifying modality & interaction heterogeneity for high-modality representation learning. *Transactions on Machine Learning Research*, 2023. Published online: `https://openreview.net/forum?id=ttzypy3kT7`.

Wei Yang Bryan Lim, Nguyen Cong Luong, Dinh Thai Hoang, Yutao Jiao, Ying-Chang Liang, Qiang Yang, Dusit Niyato, and Chunyan Miao. Federated learning in mobile edge networks: A comprehensive survey. *IEEE Communications Surveys & Tutorials*, 22(3):2031–2063, 2020.

Ze Liu, Yutong Lin, Yue Cao, Han Hu, Yixuan Wei, Zheng Zhang, Stephen Lin, and Baining Guo. Swin transformer: Hierarchical vision transformer using shifted windows. In *Proceedings of the IEEE/CVF International Conference on Computer Vision*, pp. 10012–10022, 2021.

Ziwei Liu, Ping Luo, Xiaogang Wang, and Xiaoou Tang. Deep learning face attributes in the wild. In *Proceedings of International Conference on Computer Vision (ICCV)*, December 2015.

Chris Maddison, Andriy Mnih, and Yee Whye Teh. The concrete distribution: A continuous relaxation of discrete random variables. In *Proceedings of ICLR Conference Track*, Toulon, France, 2017. Published online: `https://openreview.net/group?id=ICLR.cc/2017/conference`.

Valentino Maiorca, Luca Moschella, Antonio Norelli, Marco Fumero, Francesco Locatello, and Emanuele Rodolà. Latent space translation via semantic alignment. In *Thirty-seventh Conference on Neural Information Processing Systems*, 2023. URL `https://openreview.net/forum?id=pBa70rGHlr`.

Brendan McMahan, Eider Moore, Daniel Ramage, Seth Hampson, and Blaise Aguera y Arcas. Communication-Efficient Learning of Deep Networks from Decentralized Data. In Aarti Singh and Jerry Zhu (eds.), *Proceedings of the 20th International Conference on Artificial Intelligence and Statistics*, volume 54 of *Proceedings of Machine Learning Research*, pp. 1273–1282. PMLR, 20–22 Apr 2017. URL `https://proceedings.mlr.press/v54/mcmahan17a.html`.

David McNeely-White, Ross Beveridge, and Bruce Draper. Inception and ResNet features are (almost) equivalent. *Cognitive Systems Research*, 59:312–318, 2020.

Mazda Moayeri, Keivan Rezaei, Maziar Sanjabi, and Soheil Feizi. Text-to-concept (and back) via cross-model alignment. In *Proceedings of ICML*, pp. 25037–25060, Honolulu, HI, 2023.

Ari Morcos, Maithra Raghu, and Samy Bengio. Insights on representational similarity in neural networks with canonical correlation. In *Proceedings of NeurIPS*, Montreal, Canada, 2018. Published online: `https://papers.nips.cc/paper/2018`.

Luca Moschella, Valentino Maiorca, Marco Fumero, Antonio Norelli, Francesco Locatello, and Emanuele Rodolà. Relative representations enable zero-shot latent space communication. In *Proceedings of ICLR*, Kigali, Rwanda, 2023. Published online: `https://openreview.net/group?id=ICLR.cc/2023/Conference`.

Stefano Nolfi and Marco Mirolli (eds.). *Evolution of communication and language in embodied agents*. Springer, Berlin, Germany, 2020.

Frans Oliehoek and Christopher Amato. *A concise introduction to decentralized POMDPs*. Springer, Berlin, Germany, 2016.

Liviu Panait and Sean Luke. Cooperative multi-agent learning: The state of the art. *Autonomous Agents and Multi-Agent Systems*, 11:387–434, 2005.

Jayneel Parekh, Pegah Khayatan, Mustafa Shukor, Alasdair Newson, and Matthieu Cord. A concept-based explainability framework for large multimodal models. *Advances in Neural Information Processing Systems*, June 2024.

Alec Radford, Jong Wook Kim, Chris Hallacy, Aditya Ramesh, Gabriel Goh, Sandhini Agarwal, Girish Sastry, Amanda Askell, Pamela Mishkin, Jack Clark, Gretchen Krueger, and Ilya Sutskever. Learning transferable visual models from natural language supervision. In *Proceedings of ICML*, pp. 8748–8763, Online, 2021.

Senthooran Rajamanoharan, Tom Lieberum, Nicolas Sonnerat, Arthur Conmy, Vikrant Varma, János Kramár, and Neel Nanda. Jumping ahead: Improving reconstruction fidelity with jumprelu sparse autoencoders. *CoRR*, 2024.

Limor Raviv, Antje Meyer, and Shiri Lev-Ari. Larger communities create more systematic languages. *Proceedings of the Royal Society B: Biological Sciences*, 286(1907):20191262, 2019.

Yi Ren, Shangmin Guo, Matthieu Labeau, Shay Cohen, and Simon Kirby. Compositional languages emerge in a neural iterated learning model. In *Proceedings of ICLR*, Online, 2020. Published online: `https://openreview.net/group?id=ICLR.cc/2020/Conference`.

Tal Ridnik, Emanuel Ben-Baruch, Asaf Noy, and Lihi Zelnik. ImageNet-21K pretraining for the masses. In *Proceedings of NeurIPS Datasets and Benchmarks Track*, Online, 2021. Published online: `https://datasets-benchmarks-proceedings.neurips.cc/paper/2021`.

Mathieu Rita, Rahma Chaabouni, and Emmanuel Dupoux. "LazImpa": Lazy and impatient neural agents learn to communicate efficiently. In *Proceedings of CoNLL*, pp. 335–343, Online, 2020.

Mathieu Rita, Florian Strub, Jean-Bastien Grill, Olivier Pietquin, and Emmanuel Dupoux. On the role of population heterogeneity in emergent communication. In *Proceedings of ICLR*, Online, 2022. Published online: `https://openreview.net/group?id=ICLR.cc/2022/Conference`.

Joshua Robinson, Ching-Yao Chuang, Suvrit Sra, and Stefanie Jegelka. Contrastive learning with hard negative samples. In *Proceedings of ICLR*, Online, 2021. Proceedings at: `https://openreview.net/group?id=ICLR.cc/2021/Conference`.

Olga Russakovsky, Jia Deng, Hao Su, Jonathan Krause, Sanjeev Satheesh, Sean Ma, Zhiheng Huang, Andrej Karpathy, Aditya Khosla, Michael Bernstein, Alexander Berg, and Li Fei-Fei. ImageNet Large Scale Visual Recognition challenge. *International Journal of Computer Vision*, 115(3):211–252, 2015.

Karen Simonyan and Andrew Zisserman. Very deep convolutional networks for large-scale image recognition. In *Proceedings of ICLR Conference Track*, San Diego, CA, 2015. Published online: `http://www.iclr.cc/doku.php?id=iclr2015:main`.

Amanpreet Singh, Tushar Jain, and Sainbayar Sukhbaatar. Learning when to communicate at scale in multiagent cooperative and competitive tasks. In *Proceedings of ICLR*, New Orleans, LA, 2019. Published online: `https://openreview.net/group?id=ICLR.cc/2019/conference`.

Brian Skyrms. *Signals: Evolution, learning, and information*. Oxford University Press, Oxford, UK, 2010.

Luc Steels (ed.). *Experiments in Cultural Language Evolution*. John Benjamins, Amsterdam, the Netherlands, 2012.

Sainbayar Sukhbaatar, Arthur Szlam, and Rob Fergus. Learning multiagent communication with backpropagation. In *Proceedings of NIPS*, pp. 2244–2252, Barcelona, Spain, 2016.

Christian Szegedy, Wei Liu, Yangqing Jia, Pierre Sermanet, Scott Reed, Dragomir Anguelov, Dumitru Erhan, Vincent Vanhoucke, and Andrew Rabinovich. Going deeper with convolutions. `http://arxiv.org/abs/1409.4842`, 2014.

Adly Templeton, Tom Conerly, Jonathan Marcus, Jack Lindsey, Trenton Bricken, Brian Chen, Adam Pearce, Craig Citro, Emmanuel Ameisen, Andy Jones, Hoagy Cunningham, Nicholas L Turner, Callum McDougall, Monte MacDiarmid, C. Daniel Freeman, Theodore R. Sumers, Edward Rees, Joshua Batson, Adam Jermyn, Shan Carter, Chris Olah, and Tom Henighan. Scaling monosemanticity: Extracting interpretable features from claude 3 sonnet. *Transformer Circuits Thread*, 2024. URL `https://transformer-circuits.pub/2024/scaling-monosemanticity/index.html`.

Olivier Tieleman, Angeliki Lazaridou, Shibl Mourad, Charles Blundell, and Doina Precup. Shaping representations through communication. `https://openreview.net/pdf?id=HkzL4hR9Ym`, 2018.

Hugo Touvron, Matthieu Cord, Alexandre Sablayrolles, Gabriel Synnaeve, and Hervé Jégou. Going deeper with image transformers. In *Proceedings of the IEEE/CVF international conference on computer vision*, pp. 32–42, 2021.

Kyle Wagner, James Reggia, Juan Uriagereka, and Gerald Wilkinson. Progress in the simulation of emergent communication and language. *Adaptive Behavior*, 11(1):37–69, 2003.

Jianyu Wang, Qinghua Liu, Hao Liang, Gauri Joshi, and H Vincent Poor. Tackling the objective inconsistency problem in heterogeneous federated optimization. *Advances in neural information processing systems*, 33: 7611–7623, 2020a.

Xun Wang, Haozhi Zhang, Weilin Huang, and Matthew Scott. Cross-batch memory for embedding learning. In *Proceedings of CVPR*, pp. 6388–6397, Online, 2020b.

Ross Wightman. Pytorch image models. `https://github.com/huggingface/pytorch-image-models`, 2019.

Ronald Williams. Simple statistical gradient-following algorithms for connectionist reinforcement learning. *Machine learning*, 8(3-4):229–256, 1992.

Saining Xie, Ross Girshick, Piotr Dollár, Zhuowen Tu, and Kaiming He. Aggregated residual transformations for deep neural networks. In *Proceedings of the IEEE conference on computer vision and pattern recognition*, pp. 1492–1500, 2017.

Haofei Yu, Zhengyang Qi, Lawrence Keunho Jang, Russ Salakhutdinov, Louis-Philippe Morency, and Paul Pu Liang. MMoE: Enhancing multimodal models with mixtures of multimodal interaction experts. In *Proceedings of EMNLP*, pp. 10006–10030, Miami, (FL), 2024.

Bolei Zhou, Agata Lapedriza, Jianxiong Xiao, Antonio Torralba, and Aude Oliva. Learning deep features for scene recognition using places database. In Z. Ghahramani, M. Welling, C. Cortes, N. Lawrence, and K.Q. Weinberger (eds.), *Advances in Neural Information Processing Systems*, volume 27. Curran Associates, Inc., 2014. URL `https://proceedings.neurips.cc/paper_files/paper/2014/file/3fe94a002317b5f9259f82690aeea4cd-Paper.pdf`.

A The one-to-one referential game in pseudocode

```
initialize sender and receiver
for n training iterations do
    for batch of images b in training data do
        recdists = list()
        groundtruths = list()
        for image i in b do
            groundtruths.add(one-hot vector with 1 at i's index)
            sender receives i
            sender outputs message vector
            receiver receives message and b
            receiver processes message and each image in b to generate representations
            recdist = cosine between receiver representations of message and images in b
            recdist = softmax(recdist)
            recdists.add(recdist)
        end for
        compute cross-entropy loss CE between groundtruths and recdists
        backpropagation + update
    end for
end for
```

For the B images in a batch, the cross-entropy loss function is computed as follows:

$$\text{CE} = -\sum_{i=1}^{B}\sum_{j=1}^{B} recdists_{ij} \log(groundtruths_{ij})$$

In the population-based setup, all available senders and receivers are initialized at the beginning, and a sender and a receiver are randomly selected at each iteration of the second *for* loop.

B Using pre-trained vision modules without a communication layer

Our setup assumes that we need to connect networks that have already been pre-trained on visual tasks. An interesting question is to what extent the communication layer is adding something non-trivial to what is already encoded in the pre-trained visual representations of the networks. To assess this, we design a version of the communication game where the agents are pre-trained visual modules without any communication-specific fine-tuning.

Specifically, given two (distinct) pre-trained models that can predict image labels, we play the referential game as follows:

- sender predicts label of target image;
- receiver predicts label of all candidate images;
- if sender and receiver labels of target differ, receiver picks a random image;
- if labels coincide, the receiver picks a random image among those for which it has predicted the target label;
- the game round is successful if the receiver picks the target image.

We experimented with all the models that were trained with the same label set (ViT-B/16, Inception, ResNet152, VGG11, Swin), using 10k images for each dataset. The results are in Table 6. The models

can still communicate above chance level, but clearly communication layer training brings about a big improvement (compare to tables 2, 3, 4 and 5 above), confirming that this process is important to ensure successful referential communication across models.[14]

Dataset	**Percentage accuracy**
ImageNet (Val)	58.3 ± 21.3
ImageNet (OOD)	16.1 ± 4.3
Cifar100	9.3 ± 10.0
Places205	24.4 ± 13.0
CelebA	10.4 ± 5.2

Table 6: Percentage accuracy playing the communication game without a trained communication layer across various datasets, reported as mean ± standard deviation over all heterogeneous pairs.

C Discrete experiments

Building on intuitions from the deep net emergent communication literature, we studied whether imposing a discrete bottleneck would lead to a better, more general protocol than direct communication through a continuous channel. In a first experiment, we implemented a discrete bottleneck letting the agents exchange a one-hot vector, by optimizing it through the widely used Gumbel Softmax differentiable relaxation (Havrylov & Titov, 2017; Jang et al., 2017; Maddison et al., 2017), fixing vocabulary size (dimensionality of the message vector) to 256. Note that, when communication is discrete, a further decoder component is added to the receiver architecture, mapping the discrete messages back to the continuous space in which it can be compared to the candidate image representations.

We did not find any evidence that the discrete bottleneck helps. Not only is the discrete protocol significantly less accurate than the continuous one (Table 7), but this low performance hides any trace of better generalization capabilities (Table 8).

When generalizing a discrete communication protocol to a new agent (Fig. 6), as done for continuous messages in Section 4.3, we observe convergence to a lower accuracy at a slower pace. Still, this setup confirms even more dramatically that less time is required to train a new agent to top accuracy than is needed to retrain a larger group from scratch. Specifically, the population trained from scratch would require 23 epochs to reach its best accuracy, whereas 5 epochs are sufficient to teach a new agent an existing protocol. The population training paradigm is more stable across architectures, as with continuous messages.

In order to make sure that our negative results concerning discrete communication are not due to an unfortunate choice of hyperparameters, we repeated most experiments across a range of settings. We report here results for the more interesting population setup, but similar patterns are observed in one-to-one training. Table 9 shows that there is a small increase in accuracy when enlarging vocabulary size (compared to the results obtained with 256-dimensional messages reported in tables 7 and 8 above), but performance is still well below that of the continuous case even when using a vector as large as 8192 dimensions (compared to

[14]For technical reasons, we were not able to reproduce the Single-Class experiment for this setup. We expect however that performance would be extremely low for models that have been trained to predict the same label for all images presented in the same candidate set, as is the case with the Single-Class experiment.

	Accuracy	**Learning Time**
Homogeneous	78.2 ± 0.1	20 ± 1
Heterogeneous	71.1 ± 4.3	22 ± 2
Population	62.4 ± 3.2	23

Table 7: Percentage accuracy and learning time of agents playing the referential game with discrete messages once both agents have reached convergence. Terminology as in Table 2.

	Single-class	**Out of Domain**
Homogeneous	13.2 ± 4.1	43.2 ± 5.0
Heterogeneous	16.0 ± 6.2	29.1 ± 4.3
Population	8.9 ± 2.1	25.8 ± 4.5

Table 8: Percentage accuracy on single-class and OOD test sets for discrete communication

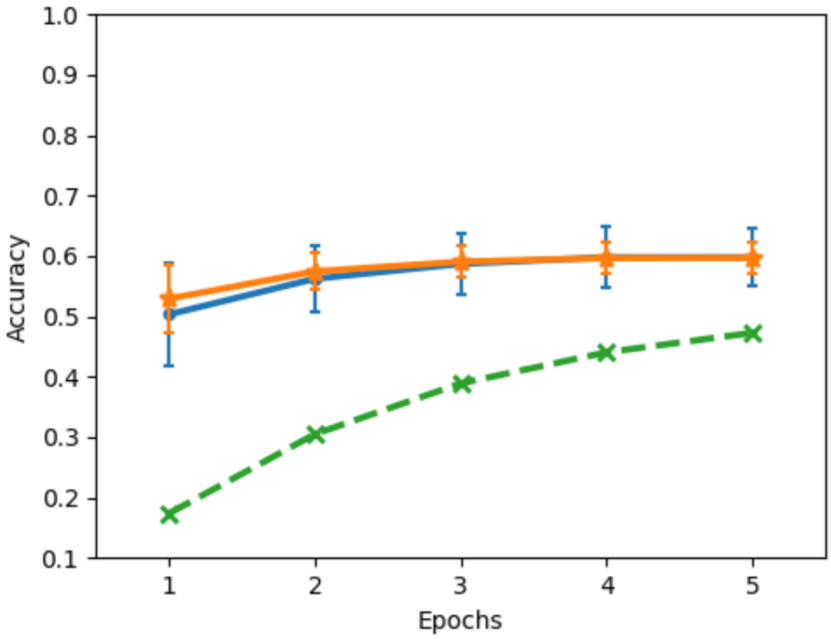

Figure 6: Test accuracy and learning speed of discrete learner agents. Blue line: learning curve on test data for learner agent added to a communicating pair, averaged across all possible heterogeneous triples. Orange line: learning curve for a learner agent added to an existing community, averaged across all possible leave-one-out cases. Vertical bars indicate standard deviation across cases. As a baseline for learning speed, the dashed green line shows the learning curve when training the whole 7x7 populations at once from scratch.

16 or 64 dimensions in the continuous case). Note that using vocabulary sizes below 256 (not shown in the table) led to failure to converge to non-random accuracy.

We also considered replacing Gumbel Softmax optimization with the commonly used policy gradient REINFORCE algorithm for fully discrete optimization (Williams, 1992). Gumbel Softmax (Table 9) proved to be the more effective training strategy. Switching to REINFORCE (Table 10) causes accuracy to drop to near-chance levels.

REINFORCE allows a straightforward implementation of multi-symbol autoregressive communication, where we let the sender and receiver produce/parse symbol sequences by replacing their communication encod-

Vocabulary size	**ImageNet1k**	**OOD**
512	62.1	26.8
1024	66.8	31.1
2048	71.7	32.1
4096	74.3	33.4
8192	78.5	35.2

Table 9: Percentage accuracy of agents evaluated on the two ImageNet-based test sets in function of vocabulary size. Agents were trained with Gumbel Softmax in a population setup.

Vocabulary size	ImageNet1k	OOD
256	5.6	3.9
512	3.4	2.4
1024	3.3	2.1
2048	2.8	1.6
4096	2.4	1.8
8192	2.2	2.1

Table 10: Percentage accuracy of agents evaluated on the two ImageNet1k test sets. Agents were trained with REINFORCE in a population setup.

	ImageNet1k	OOD
Homogeneous	84.4 ± 15.4	63.9 ± 17.7
Heterogeneous	82.2 ± 5.9	45.6 ± 12.3
Population	62.7 ± 3.4	24.9 ± 11.1

Table 11: Percentage accuracy of agents evaluated on the two ImageNet1k test sets. Agents were trained with simplicial embeddings.

ing/decoding components with a recurrent LSTM network (Hochreiter & Schmidhuber, 1997). We set maximum message length to 10 symbols. Performance of this multi-symbol approach stays capped at 1.6% accuracy, which corresponds to the random baseline.

We conjectured that the overall disappointing performance of discrete communication is due to the difficulty of optimizing agent coordination when the error gradient cannot be passed through the discrete channel. We thus tried the *simplicial* embeddings from Lavoie et al. (2023), as this approach results in nearly discrete representations while not requiring discrete-channel optimization. We applied the method on top of the continuous linear layer, which maps the vision module representation space to message space (16 dimensions). We cut the 16 dimensions into 2, 4 or 8 groups of 8, 4 or 2 vectors respectively, and apply a softmax non-linearity within those groups, before concatenating everything back to 16 dimensions. The number of groups had very little impact on results, and led to the same average performance. Accuracy with both in-domain and out-of-domain datasets is reported in Table 11, and it remains below that of plain continuous communication, without the expected boost in generalization abilities.

If using a discrete channel is considered a priority (for example, because it might lead to a more interpretable protocol), other discrete optimization techniques could also be explored, such as more advanced policy gradient methods (Francois-Lavet et al., 2018), or quantization approaches such as the one recently proposed by Carmeli et al. (2022) (although we tried something similar, with less-than-encouraging results, in Appendix Q).

D Hyperparameter search for continuous communication

Since, following standard practice, we are using the ILSVRC2012 validation partition for testing (the ILSVRC2012 test partition is not available), we rely on a separate dataset, namely Cifar100 (Krizhevsky et al., 2009), for hyperparameter tuning.

The two main hyperparameters to consider in continuous communication are the size of the continuous message, and the non-linearity applied to it. We performed multiple grid searches to determine the best and most efficient combination, through referential game experiments run on Cifar100. Table 12 shows accuracy at epochs 1 and 25 of an agent pair based on the Inception vision module.

On our validation set, all dimensions between 16 and 64 reach perfect accuracy. We thus decided to run the main experiments with both the smallest (16) and largest (64) dimensionalities in this range. We leave it to future work to explore even larger dimensionalities. We remark, however, that one of our desiderata is to keep the communication module small, and increasing dimensionality inevitably expands the size of the

Non-linearity	**Sigmoid**		**Softmax**	
Dimensions	**Epoch 1**	**Epoch 25**	**Epoch 1**	**Epoch 25**
2	5.8	14.1	13.4	12.0
4	40.2	73.8	32.6	67.3
8	97.1	99.7	94.2	98.7
16	100	100	100	99.9
32	100	100	100	100
64	100	100	100	99.8

Table 12: Grid search reporting percentage accuracies for different message dimensions and non-linearities in an Inception-to-Inception referential game on Cifar100 data.

Hyperparameters	
batch size	64
optimizer	Adam
learning rate	1e-4
max message length	1
non linearity	sigmoid
vocab size	16 / 64
receiver hidden dimension	2048
image size	384
receiver cosine temperature	0.1

Table 13: Hyperparameters for training continuous communication channels.

module. We also note here that dimensionalities smaller than 16 still manage to carry a lot of information. We are above the random chance level of $1/64 \approx 1.6\%$ even with 2 dimensions.

The sigmoid non-linearity has a small margin over softmax (clearer in the smaller dimensions, where there is no ceiling effect), and we thus pick the former for the main experiments.

E Experiment hyperparameters

All hyperparameters required to reproduce the continuous (main-text) experiments using the EGG toolkit are provided in Table 13. Hyperparameters for discrete experiments (Appendix C) are in Table 14. Table 15 has hyperparameters for the REINFORCE experiments (Appendix C). Each experiments was conducted using a single NVIDIA A30 GPU.

Hyperparameters	
batch size	64
optimizer	Adam
learning rate	1e-4
max message length	1
vocab size	8192
receiver hidden dimension	2048
image size	384
gumbel softmax temperature	5
gs temperature decay	1
update gs temp frequency	1
mimimum gs temperature	1
receiver cosine temperature	0.1

Table 14: Hyperparameters for training discrete communication channels using the Gumbel Softmax.

Hyperparameters	
batch size	64
optimizer	Adam
learning rate	1e-4
max message length	1
receiver hidden dimension	2048
image size	384
receiver cosine temperature	0.1
sender entropy coef	0.5
KL divergence coeff	0

Table 15: Hyperparameters for training discrete communication channels using REINFORCE.

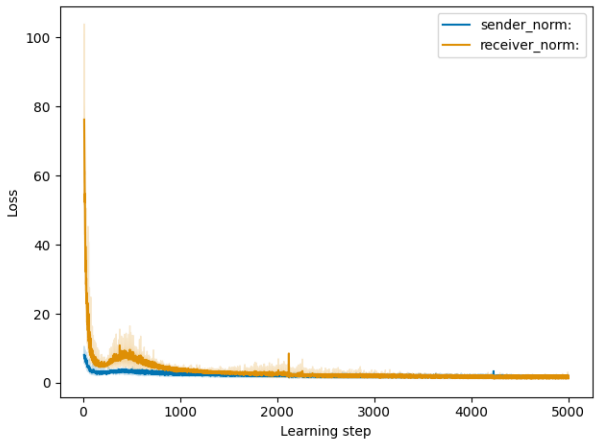

Figure 7: Higher gradient norms result in bigger optimizer steps. Despite being in a multi-agent setup, both agents stably converge. Receiver and sender lines on the plot are averages across all possible continuous one-to-one experiments.

F Gradient evolution during training

We verify convergence by providing evolution of the loss of individual continuous learners throughout training in Fig.7 (the same is true for discrete learners, around 4 times slower), also finding that receivers go through higher norm weight modification than senders during the initial stages of learning, as previously noted by Rita et al. (2022).

G Augmentations and hard distractors

We consider two training strategies commonly used in self-supervised learning: image augmentation and hard distractors. Dessì et al. (2021) showed that augmentations are crucial to develop non-degenerate protocols when training deep agents from scratch to communicate. We faithfully follow their data augmentation pipeline, using the same hyperparameters. We stochastically apply crop-and-resize, color perturbation, and random Gaussian blurring to every image.

Results for agents trained with data augmentations are presented in Table 16. In all experiments, including those that require generalizing out-of-domain, the agents trained with augmentations perform considerably worse than those trained without augmentations (compare to Tables 2 and 3 and 4 in the main text). We hypothesize that since, unlike Dessì et al. (2021), we are using pre-trained visual models that already abstract away from low-level features of the images, there is not further benefit in applying augmentation during the communication-training phase. At the same time, this phase only tunes a single layer, which implies that

	ImageNet1k	**Single-class**	**OOD**
Homogeneous	90.2 ± 6.7	30.4 ± 8.2	61.2 ± 13.7
Heterogeneous	88.7 ± 5.1	30.2 ± 2.3	53.1 ± 13.3
Population	78.8 ± 40.8	19.3 ± 39.5	41.1 ± 49.2

Table 16: Percentage accuracy of agents evaluated on the ImageNet1k test sets (64-dimensional communication channel). Agents were trained with data augmentation applied to sender and receiver inputs. No augmentation is applied at test time

	ImageNet1k	**Single-class**	**OOD**
Homogeneous	99.9 ± 0.2	47.6 ± 2.1	97.0 ± 2.2
Heterogeneous	97.1 ± 3.8	35.1 ± 9.6	68.0 ± 18.5
Population	63.7 ± 48.1	14.2 ± 8.5	30.9 ± 46.2

Table 17: Percentage accuracy of agents evaluated on the ImageNet1k-based test sets (64-dimensional communication channel). Agents were trained on batches of 64 images with low cosine distance.

the models do not have a lot of power to adapt to the augmentations. This ends up making the task harder without bringing about better abstractions skills than those already acquired during pre-training.

Another interesting idea we can borrow from self-supervised contrastive learning is that of choosing *hard* distractors at training time (Robinson et al., 2021). As we do not want to rely on data annotation, we use the *cosine* distance between pixel matrices of a target image and the other images in the training set to find near distractors (we manually checked that this simple strategy does provide intuitively similar distractors). We create batches by randomly picking an image in the Imagenet1k dataset, and adding the 63 closest images. We repeat the process throughout training. Results are found in Table 17. While agents succeed in learning communication protocols to the same degree as in the original setup, they do not outperform it. In the Single-class case, where we could expect an improvement from training on similar images, heterogeneous pairs even perform slightly worse. We thus adopt the simpler and faster random batching approach for all experiments in the main text.

H Exploiting the communication layer for zero-shot classifier transfer

Besides our primary goal to study communication between heterogeneous networks, a learned shared protocol is appealing from a representation learning perspective (Tieleman et al., 2018). We illustrate the point here by showing how, through this independently learned representation, we can perform seamless *zero-shot classifier transfer*, a task that is related to recent literature on "model stitching" (see references in the *Representation similarity and model stitching* paragraph of Related Work (Section 2) of the main article).

We consider a set of heterogeneous sender agents that have been population-trained to communicate on the ImageNet1k dataset. A single sender from the population is sampled and its output messages (64-dimensional vectors) are used to train a linear classifier on the OOD dataset classes. All agents reach good performance (Table 18) despite the fact that neither the communication layer nor the visual modules are further tuned to recognize the new out-of-domain classes.

The very same classifier is then transferred, without any further tuning, to another sender, and its OOD classification performance is evaluated. As shown in Table 18, the transfer senders, despite never having been paired up with this classifier during training, reach accuracy comparable to that of the classifier tested with the sender it was trained on (in several cases, the transfer senders even outperform the original senders, possibly thanks to the quality of their visual components).

This positive result confirms that population-training leads to a single protocol shared by all senders, and it points to the usefulness of the communication layer as a compact shared representation for visual deep nets–an opportunity to be further explored in future work.

Vision Module	Accuracy	Transfer Accuracy
VGG 11	76.7	87.6 ± 2.1
Inception	84.6	89.5 ± 3.0
ResNet 152	85.2	82.8 ± 7.3
ViT-B/16	79.84	85.6 ± 6
ViT-S/16 DINO	85.1	88.5 ± 3.0
Swin	81.8	88.7 ± 2.8
ResNet50 COCO	90.4	87.3 ± 1.9

Table 18: Percentage accuracy of a linear classifier trained to categorize objects in the OOD dataset using communication layer representations as input. Transfer accuracy is the average percentage accuracy for the same classification task when directly transfering the trained classifier to another agent from the population.

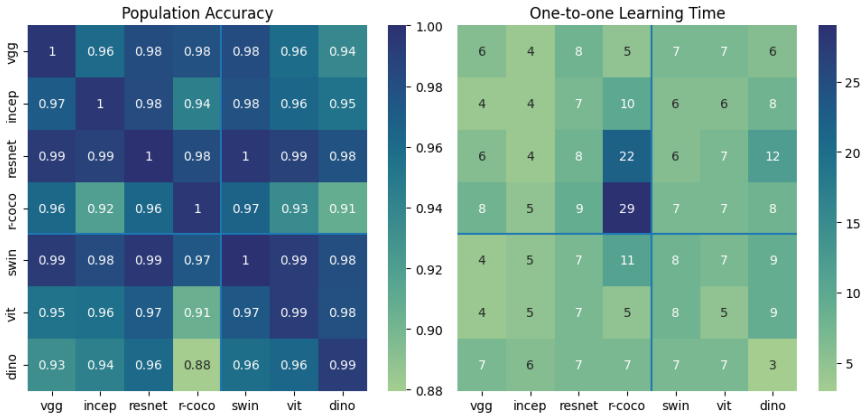

Figure 8: Pairwise population communication accuracy and heterogeneous one-to-one learning time for every visual module (16-dimensional messages). The y axis denotes senders, the x axis receivers. A line separates CNNs from attention-based architectures.

I Visual-module to visual-module analysis

In order to ensure that the high accuracy observed in terms of averaged population performance does not hide weaker communication for specific pairs, we checked every pair of agents' performance, and recorded them in Fig. 8. We present the accuracy matrix for the population setup when using 16-dimensional messages, since it is the one where we observe in general more variance from pair to pair, compared to the heterogeneous one, and to using 64-dimensional messages, where we observe a ceiling effect.

Communication accuracy is consistently high, even across different architecture types (CNNs: VGG11, Inception, ResNet, ResNet-COCO, left of the line; attention-based: Swin, ViT-B and ViT-S (DINO), right of the line) or different training paradigms (DINO was self-supervised, ResNet-COCO was pre-trained on the COCO dataset, while all other agents used supervised pre-training on the ILSVRC2012 ImageNet1k dataset). The lowest accuracies are observed when pairing ResNet-COCO (a CNN pre-trained on COCO) with either ViT-B or DINO, two attention-based architectures, suggesting a compounding effect for differences both in architecture *and* pre-training corpus.

Concerning training time, we report in Fig. 8 data for the heterogeneous one-to-one setup (population time is 28 epochs). Training times are generally low, with the two outliers involving ResNet-COCO. Note that one of these outliers is actually the homogenous ResNet-COCO-to-ResNet-COCO case, suggesting that we are observing a main effect of pre-training/communication-training corpus discrepancy, rather than issues arising when combining heterogeneous agents.

J Longer population training

We let 64-dimensional population training run for 7 times the number of epochs (175 epochs) of one-to-one pair training, so that each single agent in the population is updated as often as the one-to-one homogeneous/heterogeneous agents. Results are in Table 19.

Dataset	**Accuracy**
ImageNet (Val)	99.2 ± 1.1
ImageNet (OOD)	78.0 ± 15.3
ImageNet (Single Class)	43.6 ± 5.0
Places205	92.8 ± 6.7
CelebA	45.2 ± 24.8
Cifar100	37.6 ± 27.5

Table 19: Percentage accuracy for a population with longer training across all different datasets. Values are reported as mean ± standard deviation across models in the population.

While performance appeared to plateau, if we keep training, we observe instead non-negligible improvements across experiments (compare to tables 2, 3, 4 and 5 above). Still, in all cases except for the in-domain ImageNet set, performance still lags behind that of the heterogeneous pairs, that were trained in 1/7 of the time required to bring population performance at the level reported here.

K 16-dimensional protocol generalization to unseen datasets

We repeat the experiments reported in Table 5 with the 16-dimensional communication channel. The results (in Table 20) show that communication always remains much above random chance ($1/64 \approx 1.6\%$) in all three datasets. Nonetheless, the larger communication channel leads to better performance out of distribution, with up to 75% decrease of performance for the 16-dimensional messages in the setup where homogeneous pairs generalize from ImageNet1k to Places205.

L Sequential population training

In the main paper, we train population agents in parallel, by pairing a random sender and receiver from the whole population at each step. We explore here the alternative in which we initially train a pair of agents for a number of epochs, and then progressively let the community grow one agent at a time.

Two important hyperparameters of sequential population training are agent order and training schedule, namely how many epochs are given to each new agent before introducing the next. Concerning agent order, we tried 10 random sequences, and we report results averaged across them. Concerning training schedule, we considered two setups. In the *basic* experiment, we trained the first pair for 2 epochs, and then trained for 2 epochs more after adding each new agent (sender or receiver), for a total of 30 epochs. This is comparable to the total amount of training of the population used for the main experiments (25 epochs). In the *long* experiment, we train the initial pair for 7 epochs, and then, for each new agent we introduce, we train for 7 more epochs. This is based on the observation that pairwise convergence tends to take 7 epochs or less. In

	Cifar100	**Places205**	**CelebA**
Homogeneous	23.39 ± 2.1	25.0 ± 0.0	24.91 ± 0.15
Heterogeneous	11.78 ± 5.04	24.20 ± 0.01	15.67 ± 5.02
Population	11.09 ± 31.40	23.51 ± 42.41	14.19 ± 34.89

Table 20: Percentage accuracy on unseen datasets (Cifar100, Places205 and CelebA) for 16-dimensional messages.

this case, we are running a total of 105 epochs, closer to the training length of the experiment we report in Appendix J above (175 epochs). For both setups, we adopt a 64-dimensional communication vector.

Dataset	**Basic**	**Long**
ImageNet (Val)	94.5 ± 9.2	98.1 ± 3.1
ImageNet (OOD)	45.0 ± 22.7	72.1 ± 18.2
ImageNet (Single Class)	32.6 ± 11.1	38.4 ± 8.8
Places205	63.6 ± 26.0	91.1 ± 8.3
CelebA	33.4 ± 23.1	40.0 ± 25.2
Cifar100	27.4 ± 25.3	35.6 ± 27.7

Table 21: Percentage accuracy for two sequential training lengths on all datasets. Values are reported as mean ± standard deviation across sequence orders.

In both setups, sequential training leads to results that are inferior to those of the corresponding parallel-training experiments: cf. tables 2, 3, 4 and 5 in the main text for the *basic* results and Table 19 in Appendix J for the *long* results.

We conjecture that the problem with sequential training is that the first agents to be trained will disproportionately affect the emergent protocol, making it harder for later agents to adapt. Given also that sequential training requires more hyperparameters to tune, the takeaway here is that parallel training is the better option.

M Additional agent generalization with completely unseen models

We extended agent generalization to a set of networks that were not seen in any previous experiment or hyper-parameter search (Table 22).

Fig. 9 shows average epoch-per epoch-accuracy of those new agents, learning a protocol created by the original agents. Agents are learning a fixed communication protocol from a pair (blue) or a population (orange) of agents. These new learners (mostly based on architectures more recently developed than the ones we considered in the initial experiments) learn the protocol developed by the original agents faster and to a higher accuracy, with less variance despite having a comparable number of weights.

N Using CLIP as a visual module

We rerun all experiments adding the CLIP image encoder Radford et al. (2021) to the set of visual modules. Unlike the other networks we use, CLIP has been intentionally trained to produce visual representations that are aligned to verbal descriptions of the corresponding image contents. Images and their captions are encoded by different components, which are trained to have high similarity between their final representations, so that image representations end up aligned with text captions. Our version of CLIP uses the ViT architecture for image encoding (we use the ViT based clip model from the *"PyTorch Image Models"* library (Wightman, 2019), in it's version adapted to images of size 384x384 pixels with 16-dimensional patches).

Architecture	**Type**	**Training**	**Parameters**
ResNeXt	CNN	Supervised ImageNet1k	25.0M
LeViT	Attention	Supervised ImageNet1k and distillation	39.1M
CaiT	Attention	Supervised ImageNet1k + ImagenetV2	271.2M
DenseNet	CNN	Supervised ImageNet1k	28.7M

Table 22: Pre-trained visual architectures employed in the further agent generalization experiments. LeViT uses distillation from a model which was also trained on ImageNet1k. CaiT is trained on ImageNetV2.

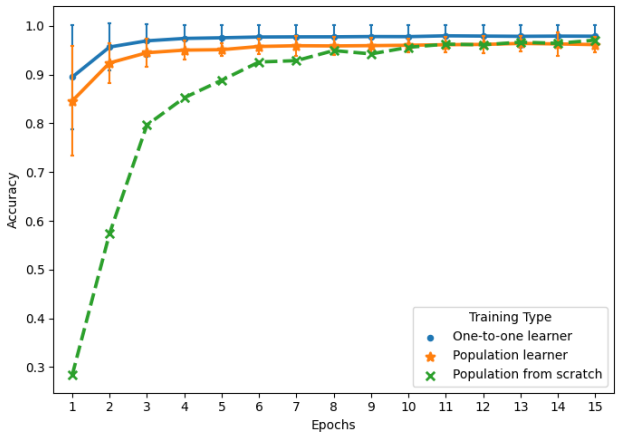

Figure 9: Test accuracy and learning speed of unseen learner agents (LeViT, CaiT, ResNeXt and DenseNet) with 64-dimensional messages. Blue line: learning curve on test data for unseen learner agent added to a communicating pair of agents from previous experiments (ResNet, ViT, VGG, Inception, DINO, Swin, ResNet COCO), averaged across all possible heterogeneous triples. Orange line: learning curve for an unseen learner agent added to an existing community, averaged across all 7 possible pre-trained agent populations. Vertical bars indicate standard deviation across cases. As a baseline for learning speed, the dashed green line shows the learning curve when training the whole original 7x7 population at once from scratch.

	ImageNet1k OOD	**Single-class**	**Cifar100**	**Places205**	**CelebA**
Homogeneous	1.0	99.83	99.46	99.98	99.94
Heterogeneous	52.70 ± 10.11	35.53 ± 9.98	44.38 ± 28.34	80.70 ± 11.91	28.28 ± 17.82
Population	62.43 ± 48.43	46.77 ± 49.90	30.35 ± 45.97	84.53 ± 36.15	30.85 ± 46.19

Table 23: Percentage accuracy on OOD datasets for pairs including a CLIP model.

Despite a strong change in training paradigm and the alignment to human language, which is a different communication protocol, results do not vary noticeably from the main results. For ImageNet1k communication, homogeneous, heterogeneous, and population setups all perform above 95% accuracy. Results are also similar to those of unimodal agents for both referent generalization (Table 23) and agent generalization (Fig. 10).

O Further SAE feature examples

Fig. 11 shows SAE features that seem to represent, respectively, 1) cups, glasses and other food containers 2) airplanes and 3) transportation and large animals. As in Section 4.4.2, the features correspond to one-hot vectors in SAE space, and we capture their semantic content by looking at the ImageNet1k images whose messages are the nearest neighbours of these vectors. Both the container feature and the airplane feature seem coherent, with little variation in the nature of the images closest to the feature. For the transportation/large animals feature, while it is understandable that vehicles and metro stations cluster together, it is less clear why large animals would also be encoded in the same feature. A tentative explanation is provided by the 9th image, where a horse and its carriage appear together. This suggests that large animals are included in this feature because they can be means of transportation, too. Alternatively, this is another example showing that SAE features are not perfectly monosemous.

Regarding the OOD images, Places205 images in the figure also tend to have a central foregrounded object, much like the ImageNet1k ones. Taking the example of the airplane feature, the closest Places205 images all have an airplane in the center of the image, exactly like the ImageNet1k images. In the case of the container and the transportation/large animals features, images from the Places205 dataset are visually more distant,

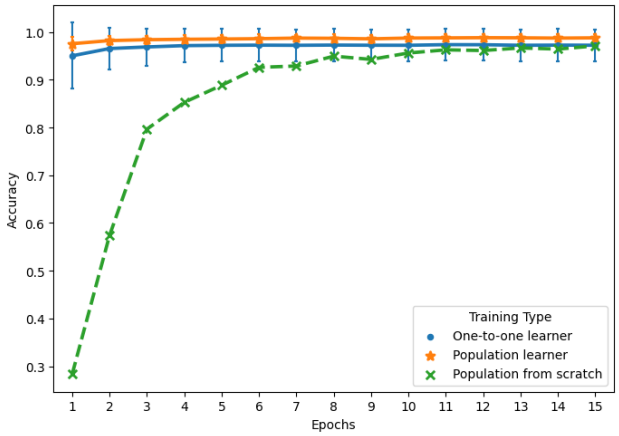

Figure 10: Test accuracy and learning speed of learner agents with 64-dimensional messages, when CLIP is added to the agent community. Blue line: learning curve on test data for learner agent added to a communicating pair including a CLIP agent, averaged across all possible heterogeneous triples. Orange line: learning curve for a learner agent added to an existing community, averaged across all possible 7 pre-trained agent populations (6 populations with CLIP, and one without, where CLIP is the learner). Vertical bars indicate standard deviation across cases. As a baseline for learning speed, the dashed green line shows the learning curve when training the original 7x7 population (no CLIP) at once from scratch.

but contain relevant objects with a clear semantic link, such as a plate for the container feature, or bus seats for transportation. For this dataset, agents seem to strongly rely on objects present in the scene, much like in the Imagenet1k case. On the other hand, the CelebA dataset results are more difficult to interpret. Celebrities within a feature appear to share common traits. For example, for the container feature, they all have black hair, and black accessories (either glasses, a hat, or a tuxedo). For the plane feature, most of them wear some kind of headgear. Despite this internal coherence, linking these pictures with the meaning we associated to the features based on ImagNet is hard, suggesting that the feature semantics have been repurposed to the very OOD nature of the dataset.

We now take a different approach. Instead of looking at images closest to a specific feature, in Fig. 12 we look for features which are closest to messages describing images from a given OOD dataset. The top feature presented in the figure is close to images from the CelebA dataset. The 10 closest ImageNet1k images to that feature all have people's faces in the foreground, and generally represent people with swimsuits. In the second case, for the feature closest to images from the Places205 dataset, the ImageNet1k images closest to that feature are all outdoor and urban settings, relevant to a dataset about places. It therefore makes sense that those features were activated the most when communicating about a given OOD image dataset, as they capture information very relevant to those datasets.

P Insights from communication errors and examples of ImageNet1k/Place205 message similarity

In this section, we look at examples of communication game errors, since some qualitative sense of what messages are expressing is also conveyed by the mistakes made by models, as shown in Fig. 13, Fig. 14 and Fig. 15. These are representative cases of when the VGG 11 sender + ViT-B/16 receiver pair that was trained in the population setup failed to converge on the target. In a large majority of them, the wrongly selected image is depicting an entity from the same class as the target (first block of examples in the figures). The fact that often the relation is conceptual rather than perceptual (as in the second example of Fig. 13, where the target is a drawing of a rocket, but the receiver picked a photograph of a rocket) confirms that agents are communicating about abstract categories, rather than low-level visual features. Of the minority of cases in which the wrongly selected image is not from the same class, some errors are relatively transparent,

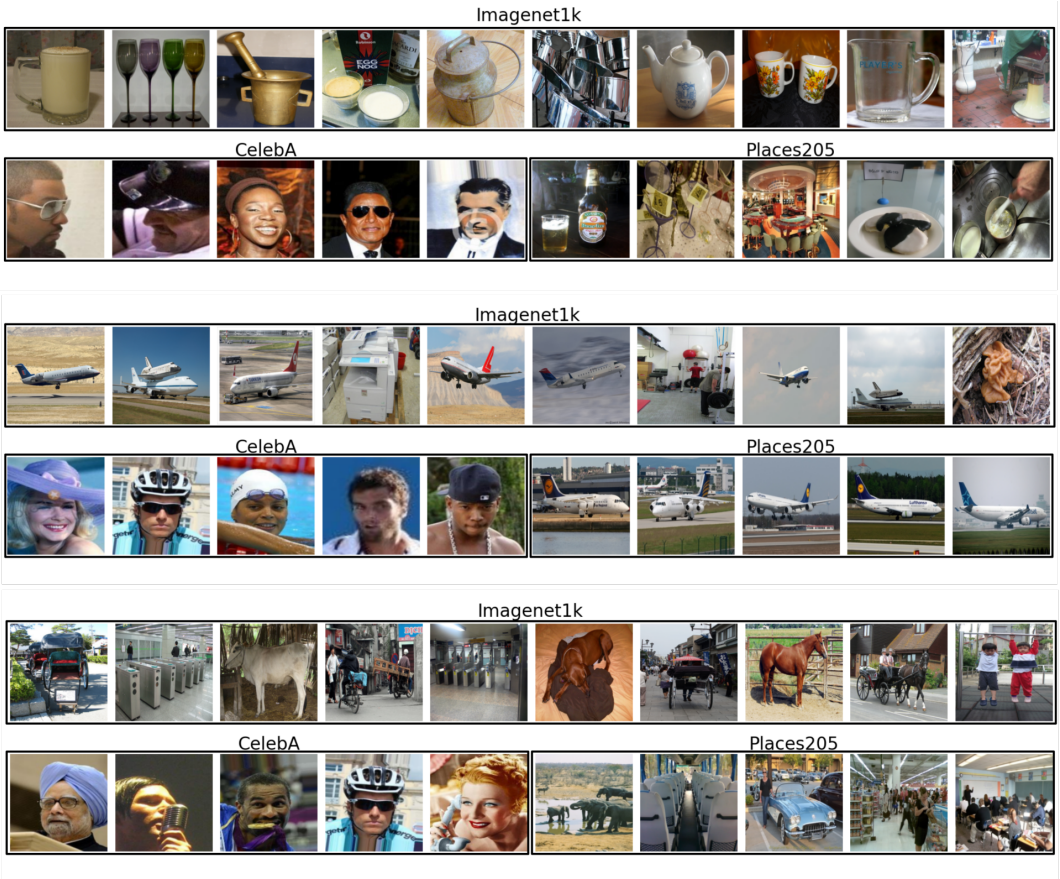

Figure 11: Three examples of SAE features and the images whose messages are closest to the feature for every dataset: Imagenet1k, CelebA and Places 205. The top feature, lines 1 and 2, could be interpreted as featuring kitchen-related containers; the second feature, lines 3 and 4, involve airplanes; and the final feature, lines 5 and 6, involve transportation and large animals. Images from CelebA an Places205 are not seen at training time by neither sender nor SAE.

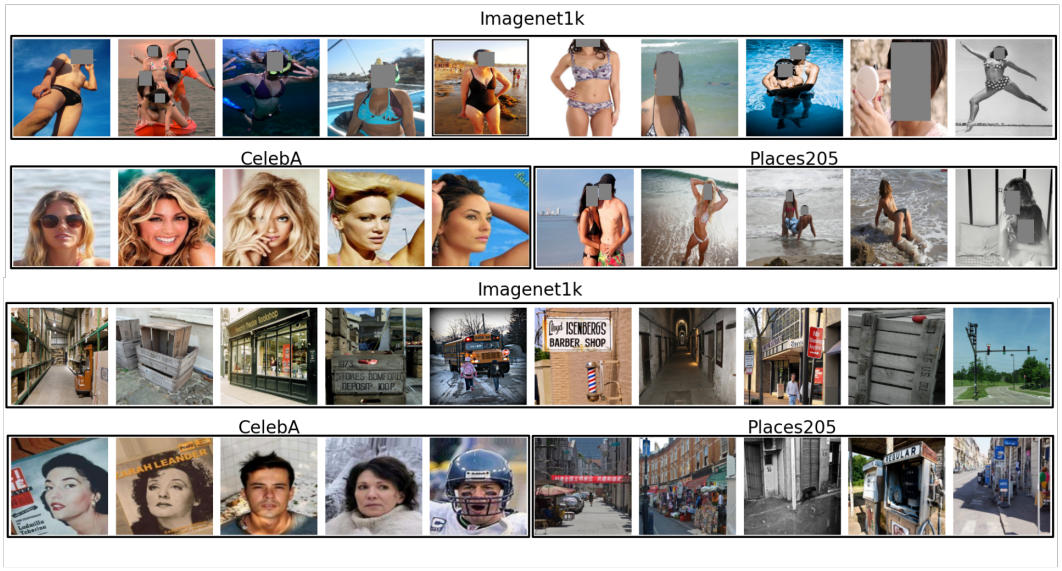

Figure 12: Two examples of features close to images from OOD datasets. The top two lines illustrate a feature closest to CelebA images, and the bottom two lines are for a feature closest to Places205 images. In each case, the closest images to the feature from each dataset are shown. We obfuscate faces of non-celebrities.

such as the ones in the second block of the figures, where we see similar shapes and textures in the target and in the wrongly picked distractor. Still, outside the frequent same-class errors, the most common case is the one illustrated by the last block of the figure, where the nature of the error is not clear.

The examples in Fig. 16, instead, shed some further light on how the agents generalize from the training dataset to out-of-distribution images. We show here just a few examples, but they illustrate general trends we qualitatively observed in a number of randomly selected cases. The top row of the figure shows target images that the receiver correctly retrieved in the Places205 dataset. For each of them, the bottom row shows the image in the ImageNet-based communication training dataset that would be retrieved by the message generated by the sender. The first example suggests that the message contains information about green and blue hues applied to natural textures. In the second example, communication probably focused on the round shape and possibly the brown-ish background color. The third case suggests, like several of the examples above, that some messages refer to high-level semantic properties, as the two images contain very different-looking instances of the same high-level concept (a vehicle). Finally, we also encounter examples, such as the last one, where it is hard to interpret what the message is encoding.

Q Discretization and other channel perturbations

In the spirit of Carmeli et al. (2022), we wondered whether we could use an easy-to-optimize continuous channel at communication training time, but then discretize the messages at inference time, thus getting the "best of both worlds".

We communication-trained the agents with dense continuous messages, but at evaluation time we discretized their messages by rounding the value of each continuous dimension in the message to either 0 or 1. On the ImageNet1k test set, performance fell to near chance levels for all investigated thresholds, in both population and one-to-one settings. Performance loss was also drastic when transforming both the 16 and 64-dimensional continuous message into a one-hot vector, using the maximum value as the "hot" value.

The continuous messages thus seem to be genuinely dense. Indeed, further analysis showed that introducing Gaussian noise (e.g., $\mu = 0$, $\sigma = 0.05$) in the messages during evaluation impacted performance negatively

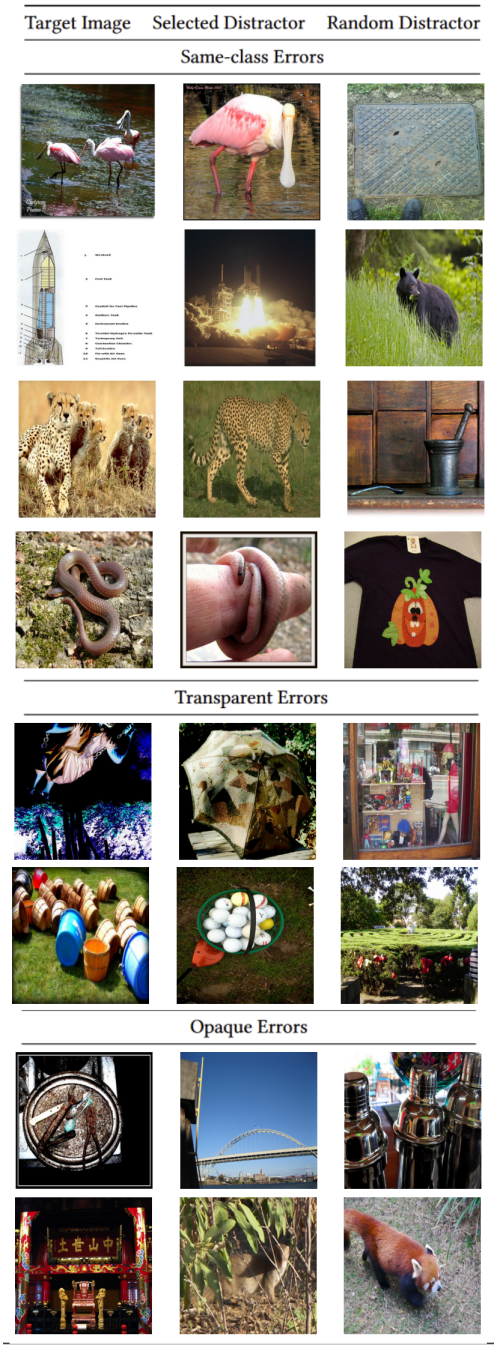

Figure 13: Examples from the ImageNet1k-based test set of mistakes made by a VGG 11 sender + ViT-B/16 receiver pair trained in the population setup. We also show an additional random distractor from the batch for context.

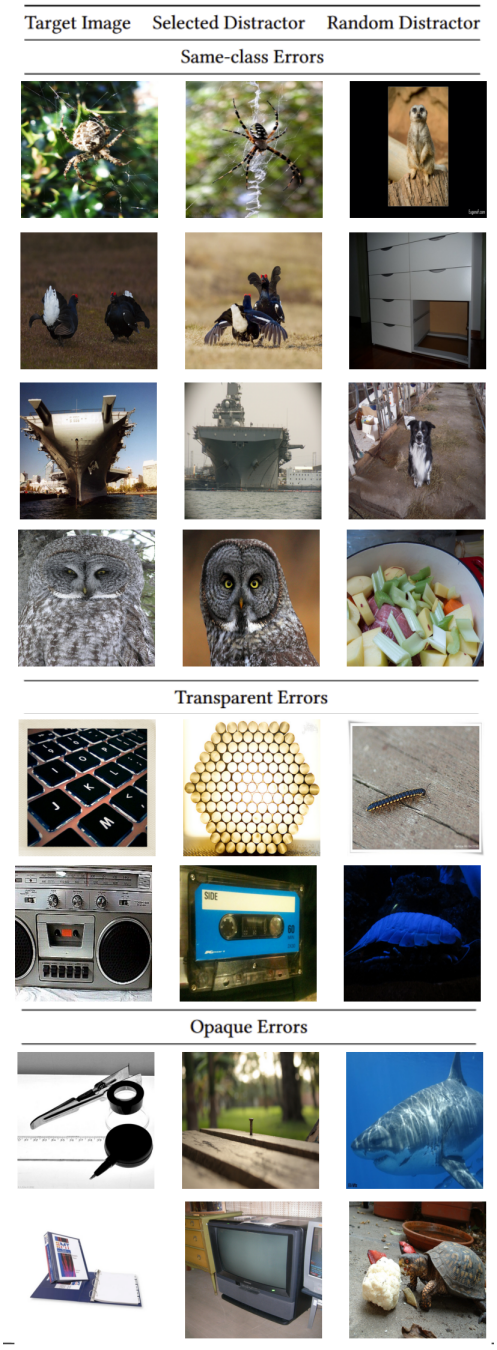

Figure 14: Examples from the ImageNet1k-based test set of mistakes made by a VGG 11 sender + ViT-B/16 receiver pair trained in the population setup. We also show an additional random distractor from the batch for context.

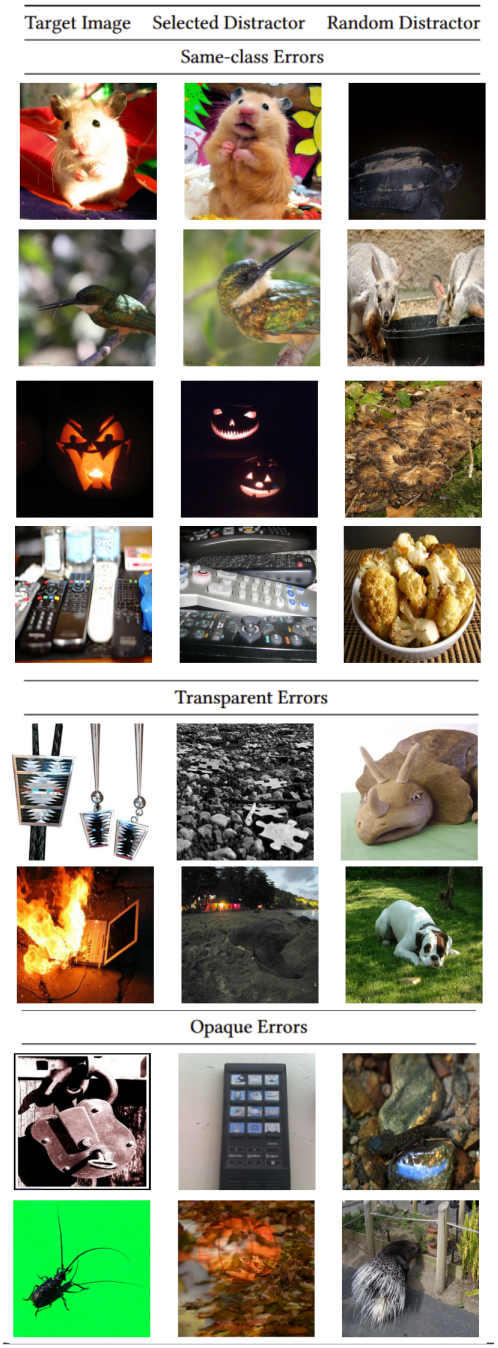

Figure 15: Examples from the ImageNet1k-based test set of mistakes made by a VGG 11 sender + ViT-B/16 receiver pair trained in the population setup. We also show an additional random distractor from the batch for context.

Figure 16: Example images correctly selected in the Places205 experiment (top row) with the images that most closely match the corresponding messages in the Imagenet1k communication-training dataset (bottom row). Agents are a VGG 11-ViT-B/16 pair.

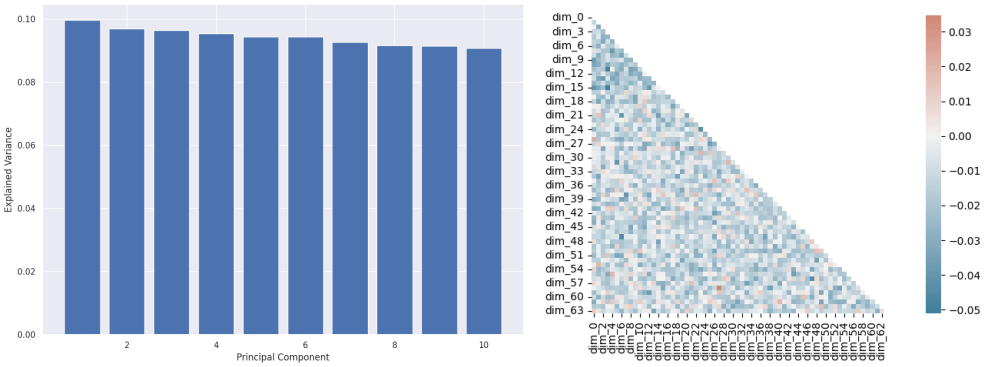

Figure 17: Explained variance for a PCA across messages (left) and correlation of the different continuous dimensions (right) from a population setup. Messages were generated by senders exposed to the ImageNet1k test set.

(22% accuracy loss). Very small changes in the message representation significantly changed the image the receiver would choose.

That information is not sparsely encoded in the continuous vector dimensions, or in some linear combinations of them, is confirmed by a PCA analysis over 64-dimensional message space.A non-linear transformation is required to disentangle the space, as performed with the SAE method in Section 4.4.2. The PCA eigenvalues are shown in Fig. 17. All PCA dimensions explain similar amounts of variance, with no dimension holding significantly more information. The figure also shows that there is no significant correlation between the original continuous vector dimensions, suggesting that they all carry independent information.